Inorganic Chemistry

Article

pubs.acs.org/IC

Iron–Amide–Sulfide and Iron–Imide–Sulfide Clusters: Heteroligated Core Environments Relevant to the Nitrogenase FeMo Cofactor

Xu-Dong Chen,[†] Wei Zhang, Jeremiah S. Duncan,[‡] and Sonny C. Lee*

Department of Chemistry, University of Waterloo, Waterloo, Ontario, Canada N2L 3G1

Supporting Information

ABSTRACT: Heteroligated cluster cores consisting of weak-field iron, strongly basic nitrogen anions, and sulfide are of interest with respect to observed and conjectured environments in the FeMo cofactor of nitrogenase. Selective syntheses have been developed to achieve such environments with *tert*-butyl-substituted amide and imide core ligands. A number of different routes were employed, including nominal ligand substitution and oxidative addition reactions, as well as novel transformations involving the combination of different cluster precursors. New cluster products include precursor $Fe_2(\mu\text{-}NH^tBu)_2[N(SiMe_3)_2]_2$ (**6**), $Fe_2(\mu\text{-}NH^tBu)_2(\mu\text{-}S)[N(SiMe_3)_2]_2$ (**7**), which has a rare confacial bitetrahedral geometry previously unknown in iron chemistry, $[Fe_2(\mu\text{-}N^tBu)(\mu\text{-}S)Cl_4]^{2-}$ (**2**), and cuboidal $[Fe_4(\mu_3\text{-}N^tBu)_3(\mu_3\text{-}S)Cl_4]^{-}$ (**8**), $[Fe_4(\mu_3\text{-}N^tBu)_2(\mu_3\text{-}S)_2Cl_4]^{2-}$ (**9**), and $[Fe_4(\mu_3\text{-}N^tBu)(\mu_3\text{-}S)_3Cl_4]^{2-}$ (**10**), as well as selenide-substituted derivatives $Fe_2(\mu\text{-}NH^tBu)_2(\mu\text{-}Se)[N(SiMe_3)_2]_2$ (**7-Se**) and $[Fe_4(\mu_3\text{-}N^tBu)(\mu_3\text{-}Se)_3Cl_4]^{2-}$ (**10-Se**). The imide–sulfide clusters complete the compositional sets $[Fe_2(\mu\text{-}N^tBu)_n(\mu\text{-}S)_{2-n}Cl_4]^{2-}$ (n = 0–2) and $[Fe_4(\mu_3\text{-}N^tBu)_n(\mu_3\text{-}S)_{4-n}Cl_4]^{z}$ (n = 0–4), represented previously only by the all-imide and all-sulfide core congeners, and they share chemical and physical properties with the parent homoleptic core species. All imide–sulfide cores are compositionally stable and show no evidence of core ligand exchange over days in solution. Beyond structural differences, the impact of mixed core ligation is most evident in redox potentials, which show progressive decreases of −435 (for z = 1−/2−) or −385 mV (for z = 2−/3−) for each replacement of sulfide by the more potent imide donor, and a corresponding effect may be expected for the interstitial heteroligand in the FeMo cofactor. Cluster **10** presents an $[Fe_4NS_3]$ core framework virtually isometric with the isostructural $[Fe_4S_3X]$ subunit of the FeMo cofactor, thus providing a synthetic structural representation for this portion of the cofactor core.

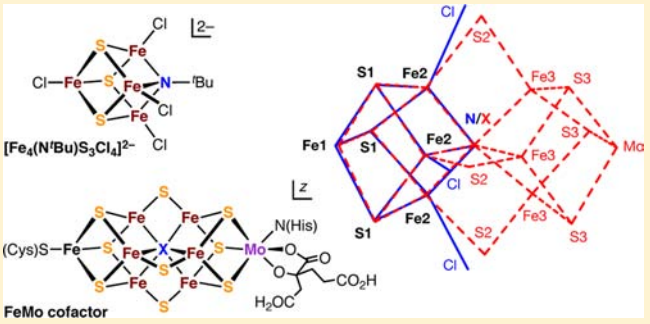

INTRODUCTION

Background. Biological nitrogen fixation is accomplished exclusively by the nitrogenase enzymes through the use of distinctive, likely related metal–sulfur cluster cofactors.[1,2] Of these, the iron–molybdenum cofactor (FeMo cofactor) of molybdenum-dependent nitrogenases is the best characterized variant.[3] Although a detailed atomic-resolution structural description exists for the FeMo cofactor[4] and the nitrogenase enzyme system has long been the focus of intense study,[1−3,5−8] the synthesis and reactivity of the cofactor cluster are poorly understood.

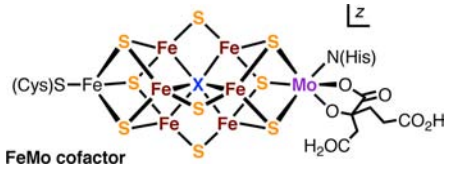

In the resting state, the FeMo cofactor possesses the core composition $[MoFe_7S_9X]^z$, where X is a monatomic ligand.[4] The core structure can be viewed as an asymmetric fusion of two different cuboidal M_4S_3X subunits, tightly integrated into a single compact cluster through the vertex-shared μ_6-X atom and three outer μ_2-sulfide bridges. The charge state z of the cluster core is uncertain, but the resting state cofactor is known to have an odd-electron count derived from some combination of high-spin Fe(II) and Fe(III) centers along with a Mo(IV) site.[7,8]

The interstitial heteroligand X is the most recent addition to the structural description of the FeMo cofactor core. A 1.16 Å resolution protein crystallographic study reported in 2002 provided the first indication of X.[4] The identity of X has been a matter of uncertainty and debate. From the original crystallographic analysis, X was deduced to be a light 2p atom, oxygen, nitrogen, or carbon, with X = N as the favored, but inconclusive, fit to observed resolution-dependent electron densities. Computational predictions of structural, electronic, and redox properties have generally supported the assignment of X = N[10−14] or, lately, C.[9] Earlier electron nuclear double resonance (ENDOR) and electron spin echo envelope modulation (ESEEM) investigations, however, were unable to detect hyperfine interactions indicative of X = ^{14}N, ^{15}N, or ^{13}C, suggesting that X is neither nitrogen nor carbon, with the caveat that X might be decoupled from the cluster

Received: August 28, 2012
Published: November 13, 2012

electron spin and therefore undetectable.[15] Very recently, Fe Kβ valence-to-core X-ray emission spectroscopy,[16] a higher 1.0 Å resolution crystallographic analysis,[17] and ESEEM study of highly enriched ^{13}C- and ^{15}N-labeled protein[17] have all produced evidence for X = C. The role of ligand X remains unestablished.

The original assignment of X = N was also prompted by the role of the cofactor in nitrogen fixation.[4] Indeed, substrate-derived nitrogenous core ligation, independent of X, has been invoked in reaction intermediates in a number of computational studies of nitrogenase mechanism.[13,18−21] The existence of such species, however, remains entirely hypothetical at this time, and no mechanistic consensus has emerged from the various theoretical efforts.[22] Recent progress has allowed spectroscopic detection of substrate-associated cofactor forms, with substrate interactions inferred to occur in the vicinity of the central iron region of the cluster, but current data allow only a limited description of the coordinated structures.[23] The molecular mechanism of cofactor action continues to be an open problem.

Cluster Models. The significance of biological nitrogen fixation and the fundamental questions surrounding the molecular inorganic chemistry of nitrogenases have made the FeMo cofactor a prominent subject of synthetic analogue efforts.[24,25] Because of the near absence of information on the FeMo cofactor in states other than the resting form, the resting state cofactor structure sets the principal benchmark for rigorous models. The synthetic problem is formidable: the core of the cofactor cluster is structurally complex, heterometallic, and heteroligated, and these salient features pose fundamental tactical challenges.

Considerable progress has been made on two of these three fronts. Heterometallic $[MFe_3S_4]$ clusters have been prepared by a number of different synthetic routes and for a variety of heterometals including M = Mo.[24] The original examples[26] predate the first crystallographic visualization of the cofactor,[27] yet they nevertheless continue to serve as highly accurate representations of the local Mo−Fe−S environment in the biological cluster.[24] More recently, a number of octanuclear Fe−S[28] and M−Fe−S[29] clusters have been attained that replicate in part or in whole the core connectivity and sulfide composition of the cofactor, although no synthetic cluster is accurate in both sulfide content and sulfide connectivity at this time.

The heteroligated Fe−S−X environment has received the least attention. Homometallic Fe−S and heterometallic M−Fe−S (M = Mo, W) clusters with heteroligated cores are known but, excluding our own studies, only for the following systems: μ_2-bridges of thiolate,[28,30] bis(trimethylsilyl)amide,[28a,31] or methoxide[32] monoanions, or chalcogenide dianions (oxide,[29a] selenide[33]), μ_3-oxide,[34] or, most recently, μ_3-, μ_4-, and μ_6-selenide.[33c,35]

We have a standing interest in the cluster chemistry of weak-field iron and strongly basic nitrogen anions (N-anions, e.g., amide, imide, nitride, and other potent nitrogen anion bases), particularly as it may relate to nitrogenase,[24,25] and we have undertaken to apply this chemistry to the construction of mixed N-anion and sulfide cores. Toward this goal, we recently communicated in brief the selective syntheses of di- and tetranuclear clusters containing iron−amide−sulfide (Fe−NHR−S) and iron−imide−sulfide (Fe−NR−S) cores, including an $[Fe_4NS_3]$ core fragment that is isometric with the corresponding $[Fe_4S_3X]$ subunit of the cofactor.[36] Our complete, detailed account of this study is presented here.

RESULTS AND DISCUSSION

Synthetic Considerations. Spontaneous self-assembly reactions constitute the primary synthetic entry to clusters containing weak-field metal centers.[24] In the simplest $M_mQ_qL_o$ cases, self-assembly involves the combination of precursors that separately provide metal ion M, bridging core ligand Q, and terminal ligand L, with the additional possibility of intervening redox interactions among the various components. To achieve heteroleptic cores, strict self-assembly would entail two core ligand components, which, for the N-anion and sulfide ligands of interest here, will have very different reactivities. In the absence of opportune pathways to kinetically favorable cluster configurations or facile equilibration to thermodynamic end points, introduction of a separate, second core ligand precursor seems unpromising for practical synthesis.

Manipulation of preorganized fragments offers a better basis for the rational, selective synthesis of more complex clusters.[24] In this matter, lessons can be drawn from the preparation of heterometallic $[MFe_3S_4]$ cubanes, which originally involved the combination of tetrathiometallates ($[MS_4]^{z-}$), $FeCl_2$, and thiolate.[26] Although the reagents are simple and the two metals are introduced as separate components, it is significant that all sulfide ligands are associated with the heterometal at the outset. While the mechanism of cluster formation is unestablished, it seems likely that the reaction proceeds through early coordination of iron to the thiometallate precursor, followed by rearrangements to give the final core stoichiometry and structure.[37,39] Other subsequent routes to heterometallic M−Fe−S clusters also rely for the most part on recognizable preorganized precursors,[24] and current progress has extended these tactics to the selective, simultaneous incorporation of both heterometal and heterochalcogenide into the $[MFe_3S_3Se]$ (M = Mo, W) cubane motif.[33c,35] Preorganization appears crucial in the selective assembly of heterometallic clusters, and we sought it here for the preparation of heteroligated cores.

The N-anion environment presents additional challenges. We have found strongly basic N-anion ligands to be more reactive than sulfide or thiolate at equivalent weak-field iron centers, requiring more restrictive reaction conditions relative to typical Fe−S systems.[39] Consequently, we developed reactions from clusters with N-anion ligands in place rather than introducing N-anion ligands to existing Fe−S systems. For similar reasons, mono(organo)-substituted N-anion ligands were employed in these first studies; although the organo-substituent distinguishes the synthetic heteroligand from proposed biochemical N-anion species, its presence greatly enhances synthetic control. The *tert*-butyl group was selected as the substituent: in addition to providing a prominent ^{1}H NMR spectroscopic handle, this tertiary alkyl group has proven to be chemically robust in these systems[40] and delivers acid−base behavior at nitrogen that approaches that of the parent unsubstituted center.[41]

Dinuclear Species. As the simplest multinuclear targets, heteroleptic dinuclear cores were the focus of our initial efforts. Two routes were developed (Scheme 1).

a. Core Ligand Substitution. Reaction of the diferric imide amine complex $Fe_2(N^tBu)_2Cl_2(NH_2{}^tBu)_2$ (**1**)[40] with 2 equiv of $(Et_4N)Cl$ followed by 1 equiv of $(Me_3Si)_2S$ leads to formation of the diferric imide−sulfide cluster $[Fe_2(N^tBu)SCl_4]^{2-}$ (**2**) in 55% isolated yield. Dinuclear **2** is the mixed core congener of the known $[Fe_2S_2Cl_4]^{2-}$ (**3**)[42] and $[Fe_2(N^tBu)_2Cl_4]^{2-}$ (**4**)[40] homoleptic core dimers. No starting material remains after reaction by NMR analysis, although a limited amount of side-product **3**, identified by UV−vis spectroscopy,[42a] occurs as a red powder during isolation; the mixed core primary product **2** is readily separated by crystallization.

This reaction is formally a core ligand substitution of imide by sulfide, and given the stability of the $[Fe_2Q_2]^{2+}$ framework under the reaction conditions, this seems a reasonable mechanistic

Scheme 1. Synthesis of Dinuclear Fe−NHR/NR−S Complexes

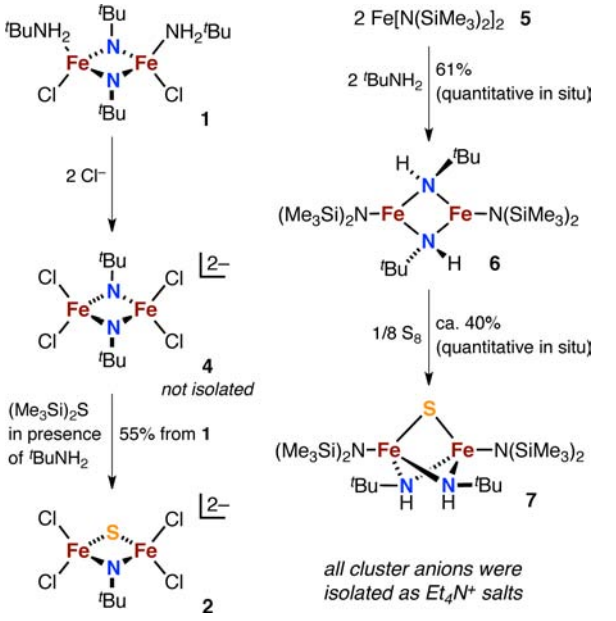

hypothesis as well. The initial step in the reaction sequence is the known displacement of amine ligands in **1** by chloride to form the tetrachloride dimer **4**.[40] Subsequent introduction of the sulfidating agent $(Me_3Si)_2S$ achieves imide substitution, presumably by silyl transfer. The displaced amine is crucial for this reaction, as treatment of isolated **4** with $(Me_3Si)_2S$ gives a complex mixture of products, while the same reaction in the presence of 1 equiv of introduced $^tBuNH_2$ smoothly forms mixed core **2**. On the basis of these observations, double silyl transfer to the bridging imide (eq 1), which would form a highly hindered, tertiary amine, does not occur. Instead, reaction stoichiometry 2 appears operative. Formation of $^tBuNH(SiMe_3)$ in eq 2 is supported by the appearance in situ of new NMR resonances at 0.03 and 1.13 ppm (CD_3CN) that exactly match the chemical shifts of authentic monosilylated amine.[43]

$$[Fe_2(N^tBu)_2Cl_4]^{2-}(\mathbf{4}) + (Me_3Si)_2S \nrightarrow [Fe_2(N^tBu)SCl_4]^{2-}(\mathbf{2}) + {}^tBuN(SiMe_3)_2 \quad (1)$$

$$[Fe_2(N^tBu)_2Cl_4]^{2-}(\mathbf{4}) + (Me_3Si)_2S + {}^tBuNH_2 \rightarrow [Fe_2(N^tBu)SCl_4]^{2-}(\mathbf{2}) + 2{}^tBuN(H)SiMe_3 \quad (2)$$

b. Oxidative Addition. Sulfide incorporation was also achieved by oxidative addition of sulfur to a ferrous amide dimer. Transamination of $Fe[N(SiMe_3)_2]_2$ (**5**)[44] with 1 equiv of $^tBuNH_2$ in benzene at 45 °C overnight gives the diferrous mixed amide dimer $Fe_2(NH^tBu)_2[N(SiMe_3)_2]_2$ (**6**). Treatment of **6** with 1 equiv of sulfur overnight in benzene leads smoothly to the oxidized diferric adduct, $Fe_2(NH^tBu)_2S[N(SiMe_3)_2]_2$ (**7**). Each conversion is quantitative by NMR assay, with isolated crystalline yields limited only by the high solubilities of the products in inert, nonpolar solvents. The two-step reaction sequence can be conducted in one pot without isolation of the intermediary dimer **6** with no loss in yield, and the end product **7** is suitable for subsequent chemistry in crude form. This system can be extended to the isostructural selenium congener **7-Se** by use of red selenium[45] in place of sulfur; in contrast with the sulfur chemistry, heating at 50 °C overnight is needed for effective addition with red selenium, and gray selenium is unreactive in this application.

In forming **6**, proton transfer occurs despite the markedly unfavorable pK_a difference between the $^tBuNH_2$ proton donor and the $(Me_3Si)_2NH$ product.[41] We suspect that this reaction is driven by additional stabilization associated with the alkylamide bridging in **6**. Further evidence for the stability of the dinuclear motif comes from the structural relationship between **6** and **7**/**7-Se**, which suggests that chalcogen addition occurs directly onto the dinuclear framework of **6**. The *tert*-butyl groups, however, are trans-disposed about the Fe_2N_2 rhomb in **6** but cis-disposed in **7**/**7-Se** (see structural discussion). Rearrangement could proceed with retention of the overall dinuclear structure through transient loss of bridging at a single *tert*-butylamide ligand, followed by nitrogen inversion of the newly terminal amide, then reformation of the bridge with the final substituent orientation. Fundamental differences in reactivity between the mixed amide **6** and the starting homoleptic silylamide **5** are evident in the sulfur addition chemistry: treatment of **5** with sulfur does not form the all-silylamide version of **7** but instead gives a product mixture that includes $Fe_4S_4[N(SiMe_3)_2]_4$ and $Fe[N(SiMe_3)_2]_3$.[46]

Cubane Clusters. Successful synthesis of diferric N-anion−sulfide cores led us to explore the preparation of higher nuclearity species. Given the stability and prevalence of the tetranuclear $[Fe_4Q_4]^q$ cubane framework, the existence of the all-sulfide[47] and all-imide[39,48,49] forms of this core, and the biological significance of the all-sulfide cluster,[47] preparation of mixed imide−sulfide cubane clusters was considered a practical and useful objective.

Weak-field $[Fe_4Q_4]^q$ cubanes can be obtained from $[Fe_2Q_2]^{2+}$ cores. Chloride-terminated cubane formation is typically triggered through external reductants (eqs 3 and 4),[39,42a] but thermally induced autoreduction (eq 5),[40] which presumably involves sacrificial oxidation of starting material, has also been observed. These routes have seen little preparative use inasmuch as self-assembly from simple components offers more efficient preparations, and the mechanism of cubane formation from dimers is unestablished. Nonetheless, the availability of N-anion, sulfide, and mixed N-anion−sulfide dinuclear cores suggested their application here as preorganized precursors in analogous transformations.

$$2[Fe_2S_2Cl_4]^{2-}(\mathbf{3}) + 2e^- \rightarrow [Fe_4S_4Cl_4]^{2-} + 4Cl^- \quad (3)$$

$$2[Fe_2(NAr)_2Cl_4]^{2-} + Zn \rightarrow [Fe_4(NAr)_4Cl_4]^{2-} + Zn^{2+} + 4Cl^- \quad (4)$$

$$[Fe_2(N^tBu)_2Cl_4]^{2-}(\mathbf{4}) \xrightarrow[\Delta]{} [Fe_4(N^tBu)_4Cl_4]^- \quad (5)$$

$$[Fe_2(N^tBu)SCl_4]^{2-}(\mathbf{2}) + 2e^- \nrightarrow [Fe_4(N^tBu)_2S_2Cl_4]^{2-} + 4Cl^- \quad (6)$$

Although direct extensions of eq 3 to the synthesis of Fe−NR−S cubanes (e.g., eq 6) resulted in poor yields and inseparable mixtures, other, novel reaction routes were successfully developed from these studies, as summarized in Scheme 2. These reactions involve the explicit combination of two different cluster reactants in most cases; in all cases, reaction yields, based on total iron content unless otherwise noted, and core composition selectivities are good to excellent, as indicated in the scheme. Details of individual syntheses follow, with hypothetical reaction stoichiometries and mechanistic issues discussed in a subsequent section.

*a. $[Fe_4(N^tBu)_3SCl_4]^-$ (**8**).* Our first indication of the existence of Fe−NR−S cubanes came from investigation of the synthesis

dx.doi.org/10.1021/ic301868m | Inorg. Chem. 2012, 51, 12891−12904

Scheme 2. Synthesis of Fe−NR−S Cubanes

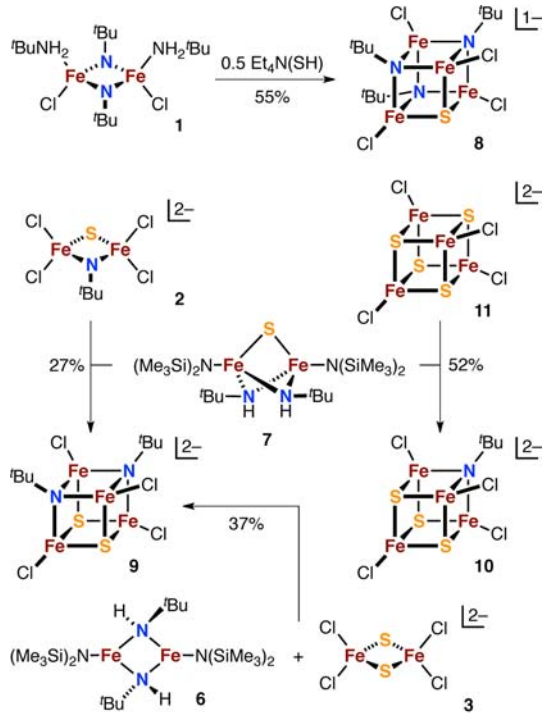

Yields and Selectivities

	isolated	in situ
8	55%	67% + trace $[Fe_4N^tBu)_4Cl_4]^-$
9 via **2** + **7**	27%	55% + trace **10**
9 via **3** + **6**	37%	54% + 14% **10** + trace **8**
10	52%	55% + 14% **9** + trace **8**

of dinuclear **2**, where the use of other sulfide sources (Na_2S, NaSH, $(Et_4N)SH$) in place of $(Me_3Si)_2S$ gave product mixtures from which imide−sulfide cubanes were identified. Further study and optimization led to reaction of **1** with 0.5 equiv of $(Et_4N)SH$,[50] which directly forms the triimide monosulfide cubane **8**. In our preliminary report,[36] twice the amount of $(Et_4N)SH$ (1 equiv) was employed, but we found inconsistent product selectivity at this stoichiometry. Our revised preparation reliably gives good yields and excellent core composition selectivity.

b. $[Fe_4(N^tBu)_2S_2Cl_4]^{2-}$ (**9**). As reported originally,[36] reaction of the imide−sulfide dimer **2** with the triply bridged amide−sulfide dimer **7** forms the diimide disulfide cubane **9**. We have developed an alternate route to this cluster via reaction of the diferrous heteroleptic amide dimer **6** with the diferric all-sulfide dimer **3**. The solution yield is comparable to that of the original reaction system, albeit with higher levels of other mixed core cubanes as side products. The principal product **9**, however, can be isolated by extraction with CH_2Cl_2 and subsequent recrystallization, and this new route is more accessible from basic starting materials.

c. $[Fe_4(N^tBu)S_3Cl_4]^{2-}$ (**10**). The final member of the imide−sulfide cubane series can be prepared by reaction of **7** with $[Fe_4S_4Cl_4]^{2-}$ (**11**).[42a,b,51] The yield in this case is calculated based on the contribution of four of the six available iron equivalents to cubane formation, as indicated later in the discussion of reaction stoichiometry. The loss of Fe−S reaction mass is supported by the accompanying formation of substantial quantities of black, insoluble, air-sensitive material that contains, by energy-dispersive X-ray microanalysis, iron and sulfur but little chlorine. The isolation of **10** is achieved by filtration to remove the insoluble matter, extraction with CH_2Cl_2 to remove the more soluble side-product **9**, and recrystallization. This reaction can be applied to preparation of the selenium analogue **10-Se** via reaction of **7-Se** with $[Fe_4Se_4Cl_4]^{2-}$ (**11-Se**).[52] As in the synthesis of **10**, a minor coproduct (not isolated) is evident in the NMR spectrum of crude **10-Se**. The position of the resonance for this species (see solution characterization section) is near that of **9**, leading to assignment of the coproduct as the diimide diselenide congener **9-Se** by analogy; the presence of **9-Se** was confirmed by electrospray ionization mass spectrometry (ESI-MS).

Structures. All new clusters were identified conclusively by single-crystal X-ray diffraction analysis. The structures are presented in Figure 1, and selected metrics for the dimers and cubanes are provided separately in Tables 1 and 2.

a. Dimers. The edge-fused bitetrahedral structure of imide−sulfide dimer **2** combines the structural features of its homoleptic congeners **3**[40] and **4**.[42b] The Fe−N and Fe−S distances are essentially the same as those in the congeners, with corresponding acute Fe−S−Fe and near 90° Fe−N−Fe angles; accordingly, the Fe···Fe separation assumes a value between the homoleptic limits. The Fe_2NS rhomb is essentially planar and the imide nitrogen center nearly so.

Likewise, the heteroleptic amide **6** can be compared against the two known homoleptic analogues, **4** ($[Fe(NSiMe_3)_2]_2$ in the solid state) and $[Fe(NPh_2)_2]_2$.[44b] The shared structural motif consists of two planar three-coordinate Fe(II) centers, each with one terminal and two bridging amide ligands, forming a planar Fe_2N_2 rhomb core. The Fe−N and Fe···Fe distances are comparable among these structures, with the Fe−N(bridge) distances shorter by 0.06 Å in **6** versus the equivalent distances in **4**. In **6**, the most basic and least hindered nitrogen donors serve as bridges, which accounts for its shorter Fe−N(bridge) distance and may explain the stability of the dimeric structure. Heteroleptic compositions have not been previously reported for ferrous bis(amides) with simple, nonchelating amide ligands.

The triply bridged, confacial bitetrahedral geometry in **7** and **7-Se**, by contrast, is new to iron chemistry, having been found previously only in a few d^{8-10} late transition metal systems.[53−56] The Fe−S distances are essentially equivalent to those observed in **2**. External comparison of Fe−N(bridge) bond lengths is difficult as symmetric bridging amide moieties are otherwise unknown in Fe(III) species.[57] Substitution by selenium in **7-Se** results in longer iron−chalcogen distances[58] but leaves the other iron−ligand distances unaffected.

b. Cubanes. The imide−sulfide cubane clusters **8**−**10** are heteroleptic core derivatives of established weak-field all-sulfide[42a,b] and all-imide[49] clusters. Equivalent structural metrics (Fe−N, Fe−S distances; Fe−N−Fe, Fe−S−Fe angles) are closely comparable across the entire $[Fe_4(N^tBu)_nS_{4-n}Cl_4]^z$ compositional range. $[Fe_4(NR)_4]$ cores more closely approach a true cubic geometry relative to $[Fe_4S_4]$ cores, which are better described as interpenetrating, concentric Fe_4 and S_4 tetrahedra; the μ_3-N and μ_3-S angles in the heteroligated cores follow similarly, with Fe−N−Fe angles approaching 90° and Fe−S−Fe angles more acute at ca. 70°. Selenium substitution in **10-Se** results in longer Fe−chalcogen bond lengths and more acute Fe−chalcogen−Fe angles, in keeping with the increased ionic radius of selenide relative to sulfide.[58]

The cubane geometries approach the highest possible idealized symmetries for their core compositions (C_{3v} for **8**,

dx.doi.org/10.1021/ic301868m | Inorg. Chem. 2012, 51, 12891−12904

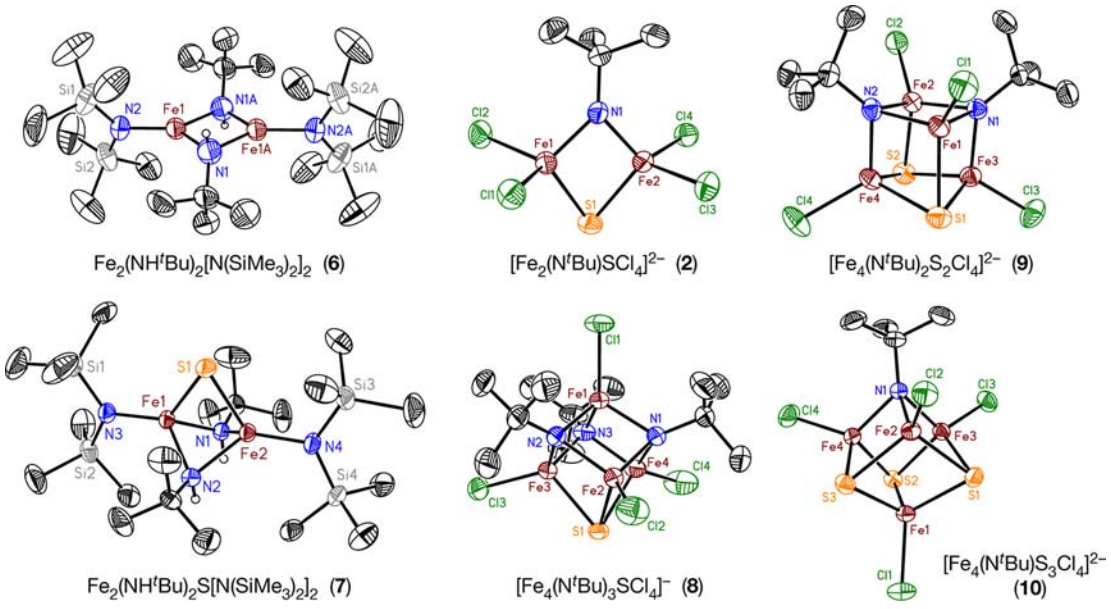

Figure 1. Cluster structures showing non-hydrogen atoms (50% probability thermal ellipsoids), amide hydrogens (small open circles), and selected atom labels. In **6**, atoms with labels ending in "A" are generated by crystallographic inversion symmetry. Selenium-containing clusters $Fe_2(NH^tBu)_2Se[N(SiMe_3)_2]_2$ (**7-Se**) and $[Fe_4(N^tBu)Se_3Cl_4]^{2-}$ (**10-Se**) are isostructural with their sulfur analogues **7** and **10**, and their structural depictions are available as Supporting Information, Figure S1.

Table 1. Selected Distances (Angstroms) and Angles (degrees) for Dinuclear Clusters[a]

	2	6	7	7-Se
Fe−N_b	1.842(5)	2.014(4)	2.054(8)	2.051(7)
Fe−Q	2.233(8)		2.234(5)	2.366(7)
Fe−Cl/N_t	2.277(10)	1.893(3)	1.882(3)	1.887(3)
Fe···Fe	2.5653(9)	2.6785(11)	2.4557(8)	2.4802(4)
N_b···N_b		3.008(7)	2.731(5)	2.727(2)
N_b···Q	3.141(4)		3.103(9)	3.218(2)
N_b−Fe−N_b		96.64(13)	83.3(4)	83.33(6)
N_b−Fe−Q	100.4(5)		92.6(3)	93.25(19)
Fe−N_b−Fe	88.3(2)	83.36(13)	73.42(12)	74.4(3)
Fe−Q−Fe	70.12(4)		66.69(4)	63.232(10)
$Fe_2(N_b)_2$ planarity[b]		0	0.460(4)	0.450(2)
Fe_2NQ planarity[b]	0.057(1)		0.410(5)	0.425(3)

[a]Arithmetic means given for multiple independent observations of the same type, with uncertainties representing the greater of either the standard deviation from the mean (almost all cases) or the largest estimated standard deviation for an individual observation. Q = S or Se, depending on complex; $N_{b/t}$ = bridging/terminal nitrogen. [b]RMS deviation from the least-squares-fitted rhomb plane.

10, **10-Se**; C_{2v} for **9**). For the rhomb faces, the donor separations are consistent by type across all core compositions, ordering as S···S > S···N > N···N, while Fe···Fe separations are more variable among the various rhomb−core combinations; these differences likely stem from core interatomic repulsions that dictate the packing of donor atoms but have less influence on Fe···Fe contacts. Of the imide−sulfide clusters characterized, **8** is one electron more oxidized than clusters **9** and **10**, but aside from a slight decrease in Fe−Cl bond length (ca. 0.03 Å), oxidation has no obvious effect on cluster structure.

Metal−imide−sulfide cubane structures are unprecedented, with the exception of the diimide disulfide core of **9**, which also occurs in nitrosyl-ligated $[Fe_4(N^tBu)_2S_2(NO)_4]^{0,1-}$ clusters.[59] The nitrosyl clusters, however, possess strong-field iron centers and differ physically and chemically from the clusters reported here; almost all equivalent core interatomic distances are appreciably shorter in the nitrosyl clusters relative to those of the weak-field counterpart **9**, as expected for low-valent clusters with strong metal−metal bonds.

c. Comparison with the FeMo cofactor. The eight-atom $[Fe_4NS_3]$ core framework of **10** is virtually isometric with the analogous $[Fe_4S_3X]$ cubane subunit of the FeMo cofactor.[4] A superposition of the relevant fragments is shown in Figure 2, with comparison metrics, averaged to C_{3v} symmetries, listed in Table 3. Corresponding core interatomic distances differ by less than 1.5% between the clusters, with the exception of a 4% deviation in the Fe1···Fe2 separation from a minor relative compression of the cofactor cluster along the idealized 3-fold axis.

The six central, X-coordinated iron sites of the FeMo cofactor tend toward trigonal monopyramidal, rather than tetrahedral, geometries.[60] If we assume that the $[Fe_4S_3X]$ portion of the cofactor reflects the intrinsic cubane geometry of the metrically congruent $[Fe_4NS_3]$ core, the superposition indicates that deformations are confined to displacement of the μ_2-S ligands away from the relaxed positions occupied by chloride in **10**. This suggests that the geometry distortions at the central iron sites arise from the need to span the vertex-fused double-cubane assembly via μ_2-S bridges.

Of course, the μ_3-imide ligand only partly replicates the μ_6 environment of X and diverges in donor atom identity if X ≠ N. These differences notwithstanding, the core metrics of the relevant subunit are in excellent agreement, and integration of a single light atom donor into an Fe−S core framework mimics a key aspect of the biological cluster. Further, the N-anion donor of the alkyl-imide ligand shares some of the electronic characteristics of a nitride ligand, and its dianionic charge state is commensurate with the formal ligand charge distribution in the $[Fe_4S_3X]$ half of the cofactor if X = C. These similarities introduce additional points of analogy between **10** and the FeMo cofactor, and comparative spectroscopic studies are in progress.[61]

Solution Identification. Solution spectroscopic data are compiled in Table 4.

All clusters in this work present characteristic, isotropically shifted resonances in their ^{1}H NMR spectra (Figure 3).

dx.doi.org/10.1021/ic301868m | *Inorg. Chem.* 2012, 51, 12891−12904

Table 2. Selected Distances (Angstroms) and Angles (degrees) for Cubane Clusters[a]

	8	9	10	10-Se
Fe−N	1.946(8)	1.95(4)	1.953(9)	1.941(17)
Fe−Q	2.306(7)	2.32(2)	2.300(9)	2.423(16)
Fe−Cl	2.197(9)	2.238(5)	2.227(8)	2.226(10)
Fe···Fe (NN face)	2.585(17)	2.6718(7)		
Fe···Fe (NQ face)	2.683(5)	2.627(9)	2.655(3)	2.678(15)
Fe···Fe (QQ face)		2.7954(9)	2.770(10)	2.797(19)
N···N	2.910(13)	2.889(5)		
N···Q	3.251(10)	3.304(4)	3.298(10)	3.411(14)
Q···Q		3.6103(16)	3.606(18)	3.86(4)
N−Fe−N	96.7(6)	94.23(7)		
N−Fe−Q	99.5(4)	101.8(5)	101.2(2)	102.0(2)
Q−Fe−Q		101.63(6)	103.4(6)	105.8(11)
Fe−N−Fe	85(2)	85.5(2)	85.64(15)	87.2(2)
Fe−Q−Fe	71.1(3)	71(2)	72.8(19)	69.3(19)
Fe_2N_2 planarity[b]	0.039(6)	0.0602(12)		
Fe_2NQ planarity[b]	0.109(10)	0.0817(11)	0.084(6)	0.090(10)
Fe_2Q_2 planarity[b]		0.2301(5)	0.168(6)	0.209(10)

[a]Arithmetic means given for multiple independent observations of the same type, with uncertainties representing the greater of either the standard deviation from the mean (almost all cases) or the largest estimated standard deviation for an individual observation. Q = S or Se, depending on complex; $N_{b/t}$ = bridging/terminal nitrogen. [b]RMS deviation from the least-squares-fitted rhomb plane.

The clusters are therefore paramagnetic under the measurement conditions, behavior consistent with the presence, fully expected from Fe−S and Fe−N-anion antecedents, of coupled high-spin iron centers with populated paramagnetic cluster spin states. The triply bridged dimers **7** and **7-Se** show inequivalent trimethylsilyl resonances, indicating restricted Fe−$N(SiMe_3)_2$ rotation, and these resonances remain unchanged on heating up to 60 °C in C_6D_6. As observed in other Fe−S/Se systems,[52] selenium analogues **7-Se**, **9-Se**, and **10-Se** display similar, but more pronounced, isotropic shifts relative to the sulfur-containing clusters.

The optical spectra of these complexes are shown in Figure 4. The heteroleptic amide complex **6** has a green color akin to that of the parent ferrous bis(amide) complex **5**,[44] while the other, sulfide-containing complexes are black in the solid state and dissolve to give deep brown solutions. The dimers have prominent features in the visible region, whereas the cubanes display only a single principal band in the ultraviolet followed by an absorption tail that extends across the entire visible region. The energy of the dominant transition in the dianionic cubane clusters increases in the order **11** (at 262 nm)[42a] < **10** < **9**. This trend is consistent with LMCT behavior that increases in energy according to decreasing first reduction potential (vide infra). The transition in **8**, which falls between those of **11** and **10**, partly follows this correlation when comparing the z = 1−/2− reduction potential of **8** against the z = 2−/3− potentials of the dianions, although the energy ordering inverts for **8** versus **10**.

Redox Behavior. All members of the $[Fe_4(N^tBu)_nS_{n-4}Cl_4]^z$ compositional series exhibit at least one well-defined (chemically or quasi-reversible) redox process in MeCN by cyclic voltammetry (Table 5, Figure 5). Quasi-reversible reduction has been linked to chloride dissociation in **11**[42a] and likely occurs in the imide−sulfide cubanes as well. Strongly basic N-anions are potent donors,[62] and as plotted in Figure 6, each replacement of sulfide by imide results in a regular, progressive negative (cathodic) shift in potential for a given redox couple across the series (ca. −0.435 mV per imide for sulfide substitution for z = 1−/2−, −0.385 mV for z = 2−/3−). Replacement of sulfide by selenide in **10-Se** leads to a +80 mV anodic shift for the 2−/3− couple to $E_{1/2}$ = −1.08 V vs SCE, whereas the corresponding potentials in $[Fe_4Q_4(SPh)_4]^{2-/3-}$ clusters (Q = S vs Se) are essentially equivalent.[63] Dinuclear imide−sulfide **2** showed only irreversible redox processes, as also observed in the homoligated congeners **3**[42a] and **4**.[40]

This analysis of heteroligand redox effects can be extrapolated to the $[Fe_4S_3X]$ and $[MoFe_3S_3X]$ cubane subunits of the FeMo cofactor. If X = C, equipartition of the formal 4− charge on the carbide ligand gives, in effect, a virtual dianionic "half-X" donor on each of the cubane subunits. Given the lower electronegativity of carbon relative to nitrogen, we expect donor strength to order as half-(μ_6-carbide) > μ_3-imide > μ_3-sulfide. Assuming charge parity for the ligation external to the cubane motifs, this trend may result in higher resting-state ferric content for the cofactor cubane subunits relative to the typical $[Fe_4S_4]^{2+}$ [47]

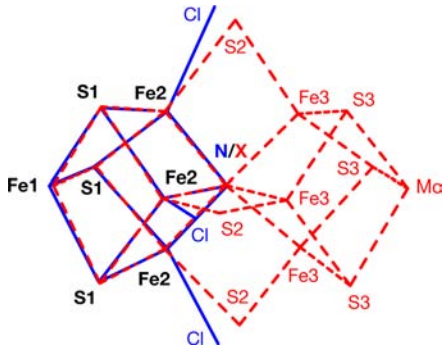

Figure 2. Superposition of the $[Fe_4NS_3]$ core of **10** (solid blue; three terminal chlorine atoms also shown) and the corresponding $[Fe_4S_3X]$ subunit of the FeMo cofactor (dashed red). Cofactor cluster G from the macromolecular structure PDB ID 1M1N (ref 4) was fitted against **10**, yielding a RMS deviation of 0.047 Å for the eight core positions.

Table 3. Comparative Mean Distances (Angstroms) and Angles (degrees) for $[Fe_4(N^tBu)S_3Cl_4]^-$ (10) and the $[Fe_4S_3X]$ Subunit of the FeMo Cofactor[a]

	10	FeMo cofactor
Fe2−N/X	1.953(9)	1.98(5)
Fe2−S1	2.305(6)	2.27(2)
Fe1−S1	2.292(11)	2.276(14)
Fe2−Cl/S2	2.226(10)	2.228(14)
Fe1···Fe2	2.770(10)	2.665(9)
Fe2···Fe2	2.655(3)	2.654(12)
N/X···S1	3.298(10)	3.28(3)
S1···S1	3.606(18)	3.62(3)
Fe1···N/X	3.517(3)	3.428(15)
S1−Fe1−S1	103.7(5)	105.3(10)
S1−Fe2−S1	102.9(6)	105.9(5)
S1−Fe2−N/X	101.2(2)	100.8(13)
Fe2−N/X−Fe2	85.65(16)	84.3(12)
Fe1−S1−Fe2	74.1(3)	71.8(6)
Fe2−S1−Fe2	70.34(10)	71.6(6)
N/X−Fe2−Cl/S2	119.8(16)	104.4(10)
S1−Fe2−Cl/S2	115(2)	120.5(16)

[a]Metrics averaged to idealized C_{3v} core symmetry using data from the structure of **10**·MeCN and the four independent FeMo cofactor structures in PDB ID 1M1N (ref 4). Arithmetic means given for multiple independent observations of the same type, with uncertainties per footnote *a* in Table 1. Atom labels correspond to those in Figure 3.

Table 4. Solution Spectroscopic Data

	^{1}H NMR:[a] δ, ppm	electronic absorption:[b] λ, nm (ε_M, L·mol^{-1}·cm^{-1})
$(Et_4N)_2[Fe_2(N^tBu)SCl_4]$ (**2**)	6.84 (9 H)[c]	254 (11 800), 271 (12 100), 360 (2600, sh), 429 (3400), 470 (2300, sh), 520 (1900, sh), 730 (400, sh)
$Fe_2(NH^tBu)_2[N(SiMe_3)_2]_2$ (**6**)	0.54 (18 H, ^{t}Bu), −1.34 (36 H, $SiMe_3$)	207 (14 500), 277 (14 500), 395 (500)
$Fe_2(NH^tBu)_2S[N(SiMe_3)_2]_2$ (**7**)	8.89 (18 H), 2.31 (18 H), 1.80 (18 H)	224 (7100), 285 (6900), 439 (4800), 570 (1200, sh)
$Fe_2(NH^tBu)_2Se[N(SiMe_3)_2]_2$ (**7-Se**)	9.31 (18 H), 3.53 (18 H), 1.68 (18 H)	240 (5700), 293 (7800), 346 (7300), 425 (4000), 610 (900, sh)
$(Et_4N)[Fe_4(N^tBu)_3SCl_4]$ (**8**)	10.51 (27 H)[c]	259 (19 600), 500 (1900, sh)
$(Et_4N)_2[Fe_4(N^tBu)_2S_2Cl_4]$ (**9**)	7.02 (18 H)[c]	235 (25 900), 510 (1900, sh)
$(Et_4N)_2[Fe_4(N^tBu)S_3Cl_4]$ (**10**)	5.51 (9 H)[c]	250 (27 300), 290 (12 100, sh), 510 (2200, sh)
$(Et_4N)_2[Fe_4(N^tBu)Se_3Cl_4]$ (**10-Se**)	5.97 (9 H)[c]	255 (49 500), 300 (20 200, sh), 490 (4200, sh)

[a] C_6D_6 or CD_3CN (neutral or ionic species, respectively), ca. 295 K. [b] *n*-Pentane or MeCN solutions (neutral or ionic species, respectively), ca. 295 K. [c] Et_4N^+ counterion resonances at ca. 3.2 and 1.2 ppm; all integral ratios are consistent with indicated cation−anion stoichiometries.

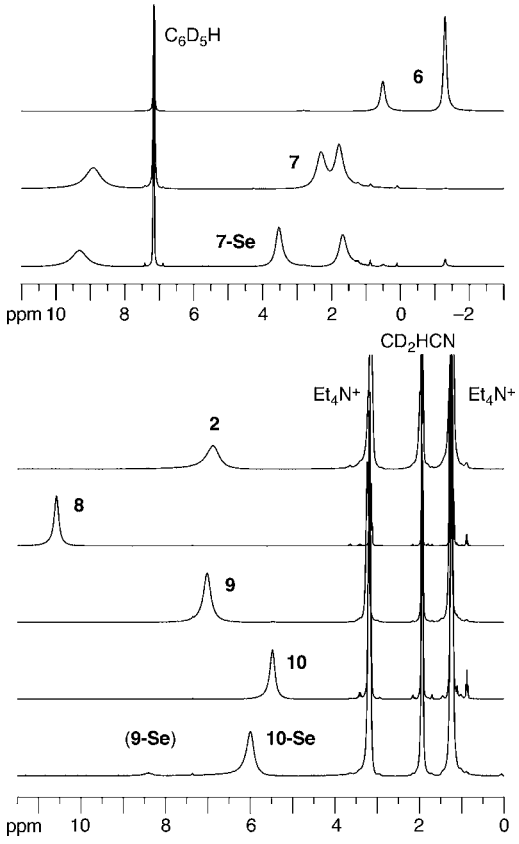

Figure 3. ^{1}H NMR spectra (295 K, 300 MHz) of amide-bridged dinuclear clusters (top, C_6D_6) and imide−sulfide clusters (bottom, CD_3CN). Trace $[Fe_4(N^tBu)_2Se_2Cl_4]^{2-}$ (**9-Se**) contaminant is detectable in the spectrum of **10-Se**.

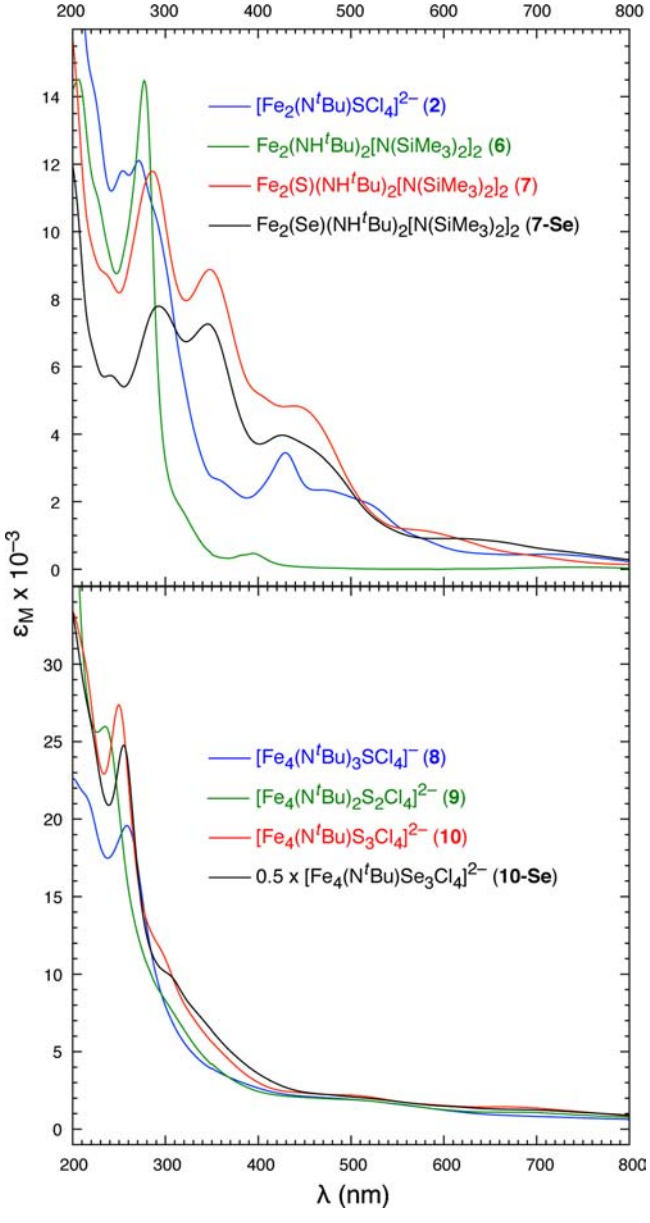

Figure 4. Solution UV−vis absorption spectra of dinuclear clusters (top) and cubane clusters (bottom) in *n*-pentane (neutral species) or MeCN (charged species). Molar absorptivity of **10-Se** is shown at half-scale to facilitate comparison with the sulfur-containing clusters.

and $[MoFe_3S_4]^{3+}$ [24a] core states obtained in synthetic reference clusters.

Electronic Properties. The magnetic properties of cubanes **8**−**10** were investigated by temperature-dependent magnetic susceptibility measurements, but anomalous, poorly reproducible results were obtained in all cases. Crystalline, analytically pure samples appear to be contaminated by trace amounts of highly magnetic material that may be linked to solution decomposition (vide infra). This contamination has precluded reliable magnetochemical analysis.

Additional electronic information was obtained by ^{57}Fe Mössbauer spectroscopy (Figure 7). Measurements in zero applied field at 130(5) K reveal symmetric patterns for clusters **9** and **10** centered at approximately δ_{av} = 0.50 mm/s, which is indistinguishable from the isomer shift of the all-sulfide **11** (δ = 0.51 mm/s at 77 K);[64] clusters **9**−**11** all possess 2Fe(II)/2Fe(III)

dx.doi.org/10.1021/ic301868m | *Inorg. Chem.* 2012, 51, 12891−12904

Table 5. Redox Potentials ($E_{1/2}$) for $[Fe_4(N^tBu)_nS_{4-n}Cl_4]^z$ Clusters (V vs SCE)[a]

	n				
z	0[b]	1	2	3	4
0/1−					+0.17
1−/2−			−0.09*	−0.53	−0.96*
2−/3−	−0.82*	−1.16*	−1.55*		

[a]Measured at 100 mV/s scan rate in MeCN with 0.1 M (n-Bu_4N)ClO_4 supporting electrolyte. Quasi-reversible processes are indicated by asterisks; remaining processes are chemically reversible. [b]Reference 42a.

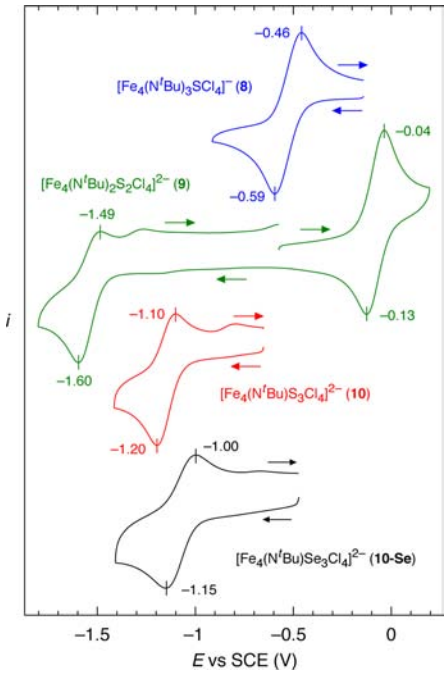

Figure 5. Cyclic voltammograms (0.1 M (n-Bu_4N)ClO_4 supporting electrolyte in MeCN, 100 mV/s scan rate) of cubane clusters. Peak potentials vs SCE and sweep directions are indicated.

formal core oxidation states. In both cases, the spectra can be analyzed as two symmetric quadrupole doublets at 1:1 intensity ratio. Because of similarities in line widths, the spectrum of **9** can be reproduced using very different combinations of isomer shifts and quadrupole splittings, and definitive parameter assignments could not be achieved. The spectrum of **8** shows only one, slightly asymmetric doublet feature; the asymmetry can be modeled as two separate symmetric doublets at 1:1 ratio, but again, individual parameter assignments must be viewed with caution. The mean isomer shift at δ_{av} = 0.43 mm/s is reduced relative to those of **9**−**11**, consistent with a more oxidized, formally 1Fe(II)/3Fe(III) core. Comparison can be made with the isoelectronic all-sulfide cubane $[Fe_4S_4(STrip)_4]^-$ (**12**, Trip =2,4,6-triisopropylphenyl),[65] the Mössbauer spectrum of which was assigned as two, equal-intensity symmetric doublets, with δ_{av} = 0.34 mm/s at 150 K; adjusting for terminal chloride ligation in **8**, which produces a larger isomer shift at the same oxidation state relative to thiolate (e.g., $[Fe_4S_4X_4]^{2-}$ at 77 K: δ = 0.51 mm/s for X = Cl vs 0.43 mm/s for X = SR),[47,64] **8** and **12** exhibit essentially equivalent isomer shifts.

The EPR behavior of the odd-electron cubane **8** was investigated at X- and Q-band frequencies in frozen 1:1 DMF/MeCN at 14 and 2 K, respectively (Figure 8). Similar signal envelopes, encompassing g = 1.9−2.1 and centered at g = 2.0,

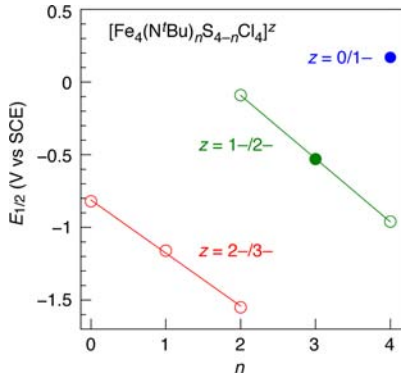

Figure 6. Redox potentials as a function of composition n in the $[Fe_4(N^tBu)_nS_{n-4}Cl_4]^z$ series. Open and filled circles indicate quasi- and chemically reversible processes, respectively, as determined by cyclic voltammetry. Lines are linear regression fits to the experimental potentials: for the z = 1−/2− couple, $E_{1/2}$ = 0.778 − 0.435n; z = 2−/3−, $E_{1/2}$ = −0.812 − 0.365n.

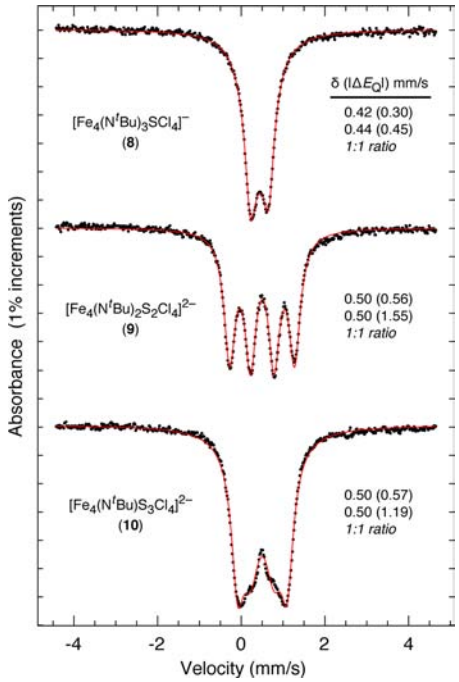

Figure 7. Mössbauer spectra (130(5) K) of polycrystalline Fe−NR−S cubane clusters. Solid red lines are spectral simulations based on the parameters indicated to the right of the spectra. Equivalent linewidths permit an alternative description of the spectrum of **9** as two equal-intensity symmetric doublets with identical $|\Delta E_Q|$ = 1.06 mm/s and δ = 0.25, 0.75 mm/s.

are obtained at both frequencies. The derivative appears to be isotropic but with a broadened, distorted aspect marked by a shoulder at lower field. The spectral correspondence at the two frequencies indicates field dependency, which excludes nitrogen hyperfine coupling as the origin of these features. The unusual line shape may arise from heterogeneity due to speciation from chloride loss, as discussed in the next section. The general spectral characteristics of **8** are consistent with S = 1/2 systems such as the isoelectronic cubane **12**, which exhibits a g-strained rhombic spectrum with g_{av} = 2.06 in toluene glass.[65]

Cubane Formation and Stability. Cluster assembly mechanisms involving weak-field metal centers are poorly understood. For the cores of interest here, the high-spin iron sites are exchange

dx.doi.org/10.1021/ic301868m | Inorg. Chem. 2012, 51, 12891−12904

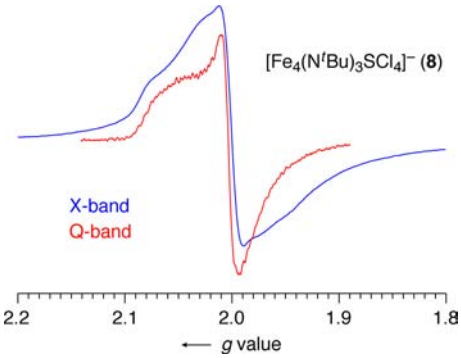

Figure 8. X- and Q-band EPR spectra (14 and 2 K, respectively; 1:1 DMF/MeCN glass) of **8**.

labile and paramagnetic, metal and core ligands are redox active, and metal coordination environments are unconstrained by chelating ancillary ligands. Mechanistic analysis under these conditions is challenging. We can make the following observations.

(1) Syntheses of the Fe−NR−S cubanes are very effective by the standards of weak-field cluster chemistry. Each of the three possible heteroleptic core compositions is accessible by its own specific reaction system, and cubane clusters form almost exclusively and in high yields (60−75% combined for all cubanes present, see Scheme 2 for tabulated yields) by total reaction assays using ^{1}H NMR spectroscopy. One product dominates (55−65%) in all cases, with selectivities for a given core composition ranging from moderate (4:1) to excellent (>30:1).

(2) By NMR assay in CD_3CN, none of the individual Fe−NR−S cubanes spontaneously transform to other congeneric core compositions over a period exceeding 1 week at millimolar concentrations and ambient temperature. Further, under the same conditions, combination of **8** and **10** does not give rise to **9** and combination of **10** and **10-Se** does not lead to mixed sulfide-selenide species. The absence of intercluster core ligand exchange and the reaction-specific outcomes noted in observation 1 demonstrate that product selectivities arise not from facile equilibration following cubane formation but from the assembly reactions themselves.

(3) The cubane clusters, however, do decompose over time in CD_3CN solution to NMR-silent products. The dianionic clusters decay most rapidly, with ca. 15% loss after 2 days for **10**. Degradation appears to require chloride dissociation inasmuch as a solution of **10** with 6 equiv of $(Et_4N)Cl$ showed no decomposition over a period of weeks. This behavior may explain the presence of magnetically active contaminants as well as the speciation observed in the EPR spectra of **8** prepared in a high-polarity, coordinating DMF/MeCN solvent system.

(4) Two preparative systems exhibit only moderate selectivity. In the synthesis of **10**, which forms with **9** in a final 4:1 ratio, time-course NMR assays revealed **10** as the sole product at the start of the reaction, with no **9** detectable until the 1-h mark. We suggest that formation of **9** arises from amide−sulfide dimer **7**, which reacts not only with starting all-sulfide cubane **11** but also with the imide−sulfide cubane product **10**. Indeed, treatment of **10** with **7** (1:1) resulted in production of **9** within 5 min as well as an immediate loss (40%) of **10** to undetected, unknown species; the disappearance of cubane clusters slowed afterward, but the ratio of **10** to **9** continued to evolve, gradually reaching 3:1 overnight. Interestingly, **9** also reacts with **7** but only with decomposition, and no other cubane congeners are formed.

By contrast, in the reaction of **6** with **3**, the minority coproduct **10** appeared immediately with main product **9** and their relative ratios remained essentially constant (ca. 1:4) through the reaction course. Dimer **6** also reacts with product **9** but does not form **10**, and only cluster disappearance is observed. The other starting species **3** does not react with **9**.

(5) Balanced reactions can be formulated from the experimental stoichiometries (eqs 7−10). Partial reduction of all-ferric reactants occurs in the majority of these reaction systems, and oxidized nitrogen coproducts are proposed based on our experience with other weak-field Fe−N-anion systems.[39,40,48,49a] However, other redox couplings are possible inasmuch as a significant fraction of the reaction mass (ca. 30% of the metal content) in these reactions goes undetected by NMR spectroscopy, and azobutane was found only at trace levels by GC analysis. We emphasize that our stoichiometries are simply working hypotheses at present.

$$2Fe_2(N^tBu)_2Cl_2(NH_2{}^tBu)_2(\mathbf{1}) + [SH]^- \rightarrow [Fe_4(N^tBu)_3SCl_4]^-(\mathbf{8}) + 0.5\,{}^tBuHN{-}NH^tBu + 4\,{}^tBuNH_2 \quad (7)$$

$$Fe_2(NH^tBu)_2S[N(SiMe_3)_2]_2(\mathbf{7}) + [Fe_2(N^tBu)SCl_4]^{2-}(\mathbf{2}) \rightarrow [Fe_4(N^tBu)_2S_2Cl_4]^{2-}(\mathbf{9}) + 0.5\,{}^tBuN{=}N^tBu + 2HN(SiMe_3)_2 \quad (8)$$

$$Fe_2(NH^tBu)_2[N(SiMe_3)_2]_2(\mathbf{6}) + [Fe_2S_2Cl_4]^{2-}(\mathbf{3}) \rightarrow [Fe_4(N^tBu)_2S_2Cl_4]^{2-}(\mathbf{9}) + 2HN(SiMe_3)_2 \quad (9)$$

$$Fe_2(NH^tBu)_2S[N(SiMe_3)_2]_2(\mathbf{7}) + [Fe_4S_4Cl_4]^{2-}(\mathbf{11}) \rightarrow [Fe_4(N^tBu)S_3Cl_4]^{2-}(\mathbf{10}) + 2HN(SiMe_3)_2 + 2FeS + 0.5\,{}^tBuN{=}N^tBu \quad (10)$$

(6) In light of the reactant structures and compositions, direct condensation of reactant-derived, preorganized cluster fragments[24] may explain the selective assembly of specific heteroleptic cubane cores. This mechanistic possibility was probed in part through labeling experiments in which the fate of chalcogenide ligands was tracked using combinations of sulfide- and selenide-containing reactants. The following mixed chalcogenide reactions were analyzed:

$$Fe_2(NH^tBu)_2Se[N(SiMe_3)_2]_2(\mathbf{7\text{-}Se}) + [Fe_2(N^tBu)SCl_4]^{2-}(\mathbf{2}) \rightarrow [Fe_4(N^tBu)_2S_nSe_{2-n}Cl_4]^{2-} \quad (11)$$

$$Fe_2(NH^tBu)_2Se[N(SiMe_3)_2]_2(\mathbf{7\text{-}Se}) + [Fe_4S_4Cl_4]^{2-}(\mathbf{11}) \rightarrow [Fe_4(N^tBu)S_nSe_{3-n}Cl_4]^{2-} \quad (12)$$

$$Fe_2(NH^tBu)_2S[N(SiMe_3)_2]_2(\mathbf{7}) + [Fe_4Se_4Cl_4]^{2-}(\mathbf{11\text{-}Se}) \rightarrow [Fe_4(N^tBu)S_nSe_{3-n}Cl_4]^{2-} \quad (13)$$

Reaction outcomes were evaluated by NMR spectroscopy, as illustrated in the representative product spectrum of reaction 12 in Figure 9. The resonances associated with mixed chalcogenide species were assigned based on their positions between the limiting chemical shifts of the known all-selenide and all-sulfide clusters; the presence of mixed cores was further confirmed by ESI-MS. Note that the product spectrum in Figure 9 is of a

dx.doi.org/10.1021/ic301868m | Inorg. Chem. 2012, 51, 12891−12904

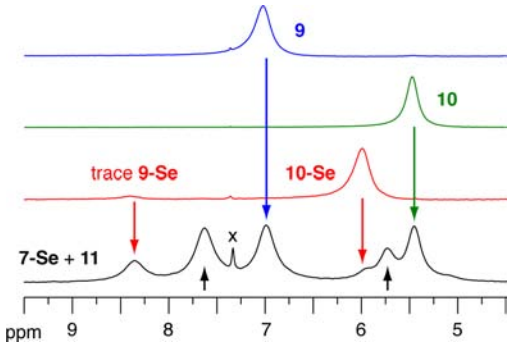

Figure 9. ^{1}H NMR assay (CD_3CN, 295 °C, 300 MHz) of 1:1 $Fe_2(NH^tBu)_2Se[N(SiMe_3)_2]_2$ (**7-Se**) and $(Et_4N)_2[Fe_4S_4Cl_4]$ (**11**) after reaction overnight (black, *tert*-butyl region). Spectra of $[Fe_4(N^tBu)_2S_2Cl_4]^{2-}$ (**9**, blue), $[Fe_4(N^tBu)S_3Cl_4]^{2-}$ (**10**, green), and $[Fe_4(N^tBu)Se_3Cl_4]^{2-}$ with trace $[Fe_4(N^tBu)_2Se_2Cl_4]^{2-}$ (**10-Se** and **9-Se**, red) are shown to illustrate corresponding product assignments in the labeling experiment. New resonances inferred for imide–selenide–sulfide cubanes $[Fe_4(N^tBu)_2SSeCl_4]^{2-}$ and $[Fe_4(N^tBu)S_nSe_{3-n}Cl_4]$ (n = 1, 2) are indicated by black arrows; for the latter species, separate resonances for the two mixed chalcogenide compositions are unresolved due to peak overlap. Residual benzene solvent signal is denoted by x.

reaction after an extended time period and is presented specifically to show the signatures of all relevant species; actual labeling experiments were assayed much earlier to reduce the effects of side reactions.

In reactions 11 and 12, all possible sulfide–selenide core compositions (n = 0–2 and 0–3, respectively) were observed within the first 5 min of reaction, whereas in reaction 13, the product distribution was dominated by the n = 0 cluster **10-Se**. The chalcogenide composition of the cubane products therefore cannot be tied to a distinct stoichiometric combination of reactant clusters in either reaction 11 or 12. The mechanistic significance of these negative observations, however, is unclear. The appearance of a compositional distribution does not necessarily exclude fragment condensation as a mechanism for cubane assembly inasmuch as the nature and chalcogen composition of critical intermediates are unknown at present; the stepwise pathways are expected to be complex due to the substantial differences between the starting structures and the final tetranuclear frameworks. In addition, the reactivity of **7** with product cubanes (observation 4) complicates the analyses, and indeed, reaction of **7-Se** with **10** forms mixed sulfide–selenide cubanes within minutes. Finally, the different outcomes of chalcogenide-inverted reactions 12 and 13 indicate that selenium is an imperfect analogue of sulfur in these systems.

SUMMARY AND OUTLOOK

We have demonstrated the construction of clusters containing weak-field iron centers and mixed N-anion–sulfide/selenide cores. The di- and tetranuclear products are obtained selectively and in good yield by specific routes that range from nominal core substitution and oxidative addition reactions to unprecedented, mechanistically complex reactions involving the combination of different precursor clusters.

With the exception of the $[Fe_4(NR)_2S_2]$ core, which has been observed previously in strong-field, nitrosyl-ligated complexes,[59] the clusters in this report possess core ligand compositions that have no counterparts for any metal. The Fe–NR–S species, however, are direct, heteroleptic core analogues of well-known Fe–S[42] and more recently reported Fe–NR[49] homoleptic core clusters, and together, they completely span the dinuclear $[Fe_2(N^tBu)_nS_{2-n}Cl_4]^{2-}$ (n = 0–2) and cuboidal $[Fe_4(N^tBu)_nS_{4-n}Cl_4]^{z-}$ (n = 0–4) compositional series.

The heteroleptic imide–sulfide core analogues share basic physical features with their homoleptic sulfide and imide congeners: clusters are constructed from tetrahedral, weak-field iron centers in +2 to +3 oxidation states; metal sites are bridged by dianionic ligands to form $[Fe_2Q_2]$ rhomb or $[Fe_4Q_4]$ cubane frameworks; and electronic structures are such that all clusters are paramagnetic at room temperature. The influence of core heteroligation is evident in metrical differences between imide and sulfide bridge geometries and in substantial, progressively incremental cathodic shifts for equivalent redox couples upon successive replacement of sulfide by imide. Substitution of *tert*-butylimide for sulfide, however, does not discernibly alter average isomer shifts in Mössbauer spectra, which appear to be governed by oxidation state and not imide–sulfide core composition.

Cluster cores constructed of weak-field iron, N-anions, and sulfide are of interest with respect to the chemistry of the nitrogenase FeMo cofactor. Related environments have been proposed in the resting state biometallocluster in the form of an interstitial X = N ligand[4,9–15] and in mechanistic intermediates involving core-bound nitrogen substrates.[13,18–22] With regard to the former proposition and the recent revision in X atom identity,[16,17] one re-examination of computational models suggests relatively limited impact in cofactor properties upon changing X = N to C.[21c] In the present work, the core $[Fe_4NS_3]$ framework of **10** is particularly noteworthy in being nearly isometric with the structurally analogous $[Fe_4S_3X]$ subunit of the FeMo cofactor.[4] We also anticipate that the pronounced effect of the imide heteroligand on cluster redox properties observed in the present systems will likely be mirrored by more potent X = C or N heterodonors in the cofactor. Detailed studies comparing the consequences of nitrogen core ligation in **10** with cofactor properties are underway,[61] as are efforts to elucidate the reactivity of N-anion heteroligands in an Fe–S environment. The development of selective synthetic approaches to mixed N-anion–sulfide cores affords a new entry point for the systematic construction of more accurate heteroligated core analogues to the FeMo cofactor.

EXPERIMENTAL SECTION

Preparation of Compounds. All operations were performed under dry, anaerobic conditions (pure N_2 atmosphere) using established protocols.[39,40] Solvents were purified by passage through desiccant columns (MBraun SPS-800) or distillation from CaH_2 (for MeCN, as well as $^tBuNH_2$ reagent), then stored over 3 Å molecular sieves or activated alumina under N_2 atmosphere. Reagents were obtained from commercial sources unless referenced to literature preparations. Solution spectroscopic data (^{1}H NMR, UV–vis) are compiled in Table 4.

$(Et_4N)_2[Fe_2(\mu\text{-}N^tBu)(\mu\text{-}S)Cl_4]$ (2). A solution of $(Et_4N)Cl$ (0.332 g, 2.0 mmol) in MeCN (6 mL) was added to a solution of $Fe_2(N^tBu)_2Cl_2(NH_2^tBu)_2$ (**1**)[40] (0.471 g, 1.0 mmol) in MeCN (30 mL) with stirring. After 4 h, $(Me_3Si)_2S$ (0.235 mL, 1.1 mmol) was added to the brownish-orange solution and the mixture stirred for an additional 12 h to afford a red-orange solution. Solvent was removed in vacuo to give a black residue that was redissolved in 1:1 MeCN/THF (12 mL) and filtered. Vapor diffusion of Et_2O into the orange-black filtrate at −30 °C produced 0.216 g of black crystals, which were isolated and rinsed with Et_2O. A second crop was obtained by volume reduction of the filtrate and further vapor diffusion with Et_2O at −30 °C (0.124 g). Total yield: 0.340 g (55%). Anal. Calcd for $C_{20}H_{49}N_3Cl_4Fe_2S$: C, 38.92; H, 8.00; N, 6.81. Found: C, 38.70; H, 8.04; N, 6.45.

dx.doi.org/10.1021/ic301868m | *Inorg. Chem.* 2012, 51, 12891–12904

Table 6. Crystallographic Data Summary for $(Et_4N)_2[Fe_2(N^tBu)SCl_4]$ (2), $Fe_2(NH^tBu)_2[N(SiMe_3)_2]_2$ (6), $Fe_2(NH^tBu)_2S[N(SiMe_3)_2]_2$ (7), $Fe_2(NH^tBu)_2Se[N(SiMe_3)_2]_2$ (7-Se), $(Et_4N)[Fe_4(N^tBu)_3SCl_4]$ (8), $(Et_4N)_2[Fe_4(N^tBu)_2S_2Cl_4]$ (9), $(Et_4N)_2[Fe_4(N^tBu)S_3Cl_4]$·MeCN (10·MeCN), and $(Et_4N)_2[Fe_4(N^tBu)Se_3Cl_4]$ (10-Se)[a]

	2	6	7	7-Se
formula	$C_{20}H_{49}Cl_4Fe_2N_3S$	$C_{20}H_{56}Fe_2N_4Si_4$	$C_{20}H_{56}Fe_2N_4SSi_4$	$C_{20}H_{56}Fe_2N_4SeSi_4$
fw	617.18	576.75	608.81	655.71
space group	$P2_1/n$ (no. 14)	$P2_1/c$ (no. 14)	$P2_1/n$ (no. 14)	$P2_1/n$ (no. 14)
Z	4	2	4	4
a, Å	9.3855(3)	11.7818(7)	16.4939(8)	16.4943(6)
b, Å	15.6669(8)	9.5043(6)	9.0249(5)	9.0935(3)
c, Å	20.7398(11)	15.9211(8)	23.5935(13)	23.5967(8)
β, deg	95.827(3)	102.368(3)	101.945(2)	91.5564(11)
V, (Å^3)	3033.9(2)	1741.4(2)	3436.0(3)	3466.6(2)
θ_{max}, deg	26.00	23.97	26.09	30.05
total data,[b] %	99.8	99.8	98.5	99.8
R_1 (wR_2),[c] %	5.34 (13.31)	4.84 (12.38)	6.04 (10.53)	3.11 (7.50)
S[d]	1.031	1.062	1.027	1.018
	8	9	10·MeCN	10-Se
formula	$C_{24}H_{58}Cl_4Fe_4N_4S_2$	$C_{20}H_{47}Cl_4Fe_4N_4S$	$C_{22}H_{52}Cl_4Fe_4N_4S_3$	$C_{20}H_{49}Cl_4Fe_4N_3Se_3$
fw	740.88	832.06	834.06	933.70
space group	$C2/c$ (no. 15)	$P2_1/c$ (no. 14)	$Pca2_1$ (no. 29)	$P2_12_12_1$ (no. 19)
Z	8	4	4	4
a, Å	23.4155(10)	17.8185(12)	26.4805(11)	11.5384(12)
b, Å	20.7305(9)	11.3121(7)	10.7835(4)	14.1705(15)
c, Å	17.8411(13)	22.1301(14)	12.7847(5)	21.395(2)
β, deg	130.1660(10)	108.7950(10)	90	90
V, (Å^3)	6618.0(6)	4222.8(5)	3650.7(2)	3498.3(6)
θ_{max}, deg	30.50	28.00	30.05	25.00
total data,[b] %	99.4	99.9	99.7	99.8
R_1 (wR_2),[c] %	3.30 (7.22)	4.98 (10.20)	3.79 (8.05)	3.36 (6.86)
S[d]	1.023	0.978	1.072	0.986

[a]Data collected at T = 200(2) K using Φ and ω scans with graphite-monochromatized Mo Kα radiation (λ = 0.71073 Å). [b]Percent completeness of (unique) data collection within the θ_{max} limit. [c]Calculated for $I > 2\sigma(I)$: $R_1 = \Sigma||F_o| - |F_c||/\Sigma|F_o|$, $wR_2 = \{\Sigma[w(F_o^2 - F_c^2)^2]/\Sigma[w(F_o^2)^2]\}^{1/2}$. [d]$S$ = goodness of fit = $\{\Sigma[w(F_o^2 - F_c^2)^2]/(n - p)\}^{1/2}$, where n is the number of reflections and p is the number of parameters refined.

$Fe_2(\mu\text{-}NH^tBu)_2[N(SiMe_3)_2]_2$ (6). A green solution of $Fe[N(SiMe_3)_2]_2$ (**5**,[44a,48] 0.301 g, 0.8 mmol) and $^tBuNH_2$ (0.084 mL, 0.8 mmol) in benzene (20 mL) was heated at 45 °C for 12 h to give a dark green solution. Solvent was removed in vacuo and the dried material redissolved in *n*-pentane, filtered, concentrated in vacuo, and equilibrated with hexamethyldisiloxane (HMDSO) by vapor diffusion at −20 °C to yield dark green crystals (0.275 g, 61%). Anal. Calcd for $C_{20}H_{56}Fe_2N_4Si_2$: C, 41.65; H, 9.79; N, 9.71. Found: C, 41.71; H, 9.74; N, 9.51.

$Fe_2(\mu\text{-}NH^tBu)_2(\mu\text{-}S)[N(SiMe_3)_2]_2$ (7). A light green solution of $^tBuNH_2$ (0.585 g, 8.0 mmol) and **5**[44a,48] (3.000 g, 8.0 mmol) in benzene (30 mL) was heated at 45 °C overnight (ca. 12 h). The resulting dark green solution was allowed to cool to ambient temperature, and sulfur (0.155 g, 0.6 mmol of S_8) was added with additional benzene washes (10 mL) to ensure complete transfer. The solution color changed to dark green-brown immediately and continued to deepen as the reaction progressed. The mixture was stirred 2 days at room temperature and then filtered through diatomaceous earth to remove excess sulfur. The dark yellow-black filtrate was taken to dryness in vacuo, leaving the product as a dark brown, glassy solid (2.089 g isolated, 86%). This crude material is sufficiently pure for preparative use, but it can be recrystallized by *n*-pentane/HMDSO vapor diffusion at −20 °C to give large black crystals (ca. 40% yield from three crops). Anal. Calcd for $C_{20}H_{56}Fe_2N_4SSi_4$: C, 39.46; H, 9.27; N, 9.20. Found: C, 39.78; H, 9.43; N, 9.26.

$Fe_2(\mu\text{-}NH^tBu)_2(\mu\text{-}Se)[N(SiMe_3)_2]_2$ (7-Se). A benzene solution (30 mL) of $^tBuNH_2$ (0.420 mL, 4.0 mmol) and **5**[44a,48] (1.506 g, 4.0 mmol) was stirred at 45 °C for 8 h. The dark green solution was allowed to cool to ambient temperature, red selenium[45] (0.189 g, 2.4 mmol) was added, and the mixture was stirred at 45 °C for a further 12 h to form a black solution. The crude product was isolated by solvent removal in vacuo and crystallized by dissolution in *n*-pentane (12 mL), filtration, and equilibration with HMDSO via vapor diffusion at −20 °C. Black crystals of **7-Se** were collected, rinsed with cold HMDSO, and dried in vacuo. Yield: 0.588 g (45%). Anal. Calcd for $C_{20}H_{56}Fe_2N_4SeSi_4$: C, 36.64; H, 8.61; N, 8.54. Found: C, 36.31; H, 8.25; N, 8.37.

$(Et_4N)[Fe_4(\mu_3\text{-}N^tBu)_3(\mu_3\text{-}S)Cl_4]$ (8). Solid $(Et_4N)SH$[50] (0.082 g, 0.5 mmol) was added to a solution of **1**[40] (0.471 g, 1.0 mmol) in THF (30 mL), and the mixture was stirred for 12 h. The resulting black solution was allowed to stand at −30 °C for 20 h and then filtered through diatomaceous earth, and the volume was reduced to 20 mL. Vapor diffusion of *n*-pentane at −20 °C gave black crystalline **8** (0.202 g, 55%). ESI-MS (MeCN, M = $C_{12}H_{27}Fe_4Cl_4N_3S$): m/z 611 $[M]^-$. Anal. Calcd for $C_{20}H_{47}Cl_4Fe_4N_4S$: C, 32.42; H, 6.39; N, 7.56. Found: C, 32.21; H, 6.20; N, 7.42.

$(Et_4N)_2[Fe_4(\mu_3\text{-}N^tBu)_2(\mu_3\text{-}S)_2Cl_4]$ (9). *Method A.* Solid **7** (0.122 g, 0.2 mmol) was added to **2** (0.123 g, 0.2 mmol) in CH_3CN (12 mL). The solution was stirred for 8 h; then the volume was reduced and diluted with THF to form a black precipitate (117 mg) that was isolated by filtration. Recrystallization by CH_3CN/Et_2O vapor diffusion at −20 °C afforded black microcrystalline material (65 mg), which was further rinsed with CH_2Cl_2 to give 45 mg (27%) of pure **9**. ESI-MS (MeCN, M = $C_8H_{18}Fe_4Cl_4N_2S_2$): m/z 702 $[M + Et_4N]^-$, 572, $[M]^-$, 567 $[M - Cl + O_2]^-$, 286 $[M]^{2-}$. Anal. Calcd for $C_{24}H_{58}Cl_4Fe_4N_4S_2$: C, 34.64; H, 7.03; N, 6.73. Found: C, 34.45; H, 6.96; N, 6.55.

Method B. To a solution of $(Et_4N)_2[Fe_2S_2Cl_4]$ (**3**,[42c] 0.223 g, 0.4 mmol) in CH_3CN (15 mL) was added **6** (0.216 g, 0.4 mmol) in THF (15 mL) with stirring. After 12 h, the reaction solution was filtered through diatomaceous earth and the solvent removed in vacuo. The resulting black oil was dissolved in CH_2Cl_2 (15 mL) and filtered, and the solvent was again removed in vacuo to leave a black oil, from

dx.doi.org/10.1021/ic301868m | Inorg. Chem. 2012, 51, 12891−12904

which black, platy crystals were obtained by CH_3CN/Et_2O vapor diffusion at −20 °C. Yield: 0.124 g (37%). The properties of this material are identical with those of the product from Method A.

$(Et_4N)_2[Fe_4(\mu_3\text{-}N^tBu)(\mu_3\text{-}S)_3Cl_4]$ (10). A solution of **7** (0.243 g, 0.4 mmol) in THF (30 mL) was added to a solution of $(Et_4N)_2[Fe_4S_4Cl_4]$ (**11**,[42a,51] 0.301 g, 0.4 mmol) in CH_3CN (30 mL). The reaction mixture was stirred for 8 h and filtered through diatomaceous earth to remove copious black precipitate. The solvent was removed under vacuum to afford a black oil, which was treated with CH_2Cl_2 (20 mL) to give black, microcrystalline product that was isolated by filtration. Recrystallization by CH_3CN/Et_2O vapor diffusion at −20 °C yielded 0.165 g (52%) of pure **10** as black, acicular crystals. ESI-MS (MeCN, M = $C_4H_9Fe_4Cl_4NS_3$): *m/z* 663 $[M + Et_4N]^-$, 533 $[M]^-$, 528 $[M - Cl + O_2]^-$, 266.5 $[M]^{2-}$. Anal. Calcd for $C_{20}H_{49}Cl_4Fe_4N_3S_3$: C, 30.29; H, 6.23; N, 5.30. Found: C, 30.11; H, 6.19; N, 5.06.

$(Et_4N)_2[Fe_4(\mu_3\text{-}N^tBu)(\mu_3\text{-}Se)_3Cl_4]$ (10-Se). A solution of **7** (0.243 g, 0.4 mmol) in THF (30 mL) was added to a solution of $(Et_4N)_2[Fe_4Se_4Cl_4]$ (**11-Se**)[52] (0.412 g, 0.4 mmol) in CH_3CN (30 mL). The mixture was stirred for 8 h and then filtered through diatomaceous earth to remove copious black precipitate. The black filtrate was evaporated under vacuum to leave a black solid, which was washed with CH_2Cl_2 (4 × 5 mL) to form black, microcrystalline material. Recrystallization by CH_3CN/Et_2O vapor diffusion at −20 °C gave 0.108 g (22%) of pure **10-Se** as black, platy crystals. Anal. Calcd for $C_{20}H_{49}Cl_4Fe_4N_3Se_3$: C, 25.73; H, 5.29; N, 4.50. Found: C, 25.95; H, 5.32; N, 4.34. ESI-MS of the crude reaction solution revealed both **10-Se** and **9-Se** (MeCN): *m/z* 805 $[Fe_4(N^tBu)Se_3Cl_4 + Et_4N]^-$, 796 $[Fe_4(N^tBu)_2Se_2Cl_4 + Et_4N]^-$, 666 $[Fe_4(N^tBu)_2Se_2Cl_4]^-$, 657 $[Fe_4(N^tBu)_3SeCl_4]^-$, 337 $[Fe_4(N^tBu)Se_3Cl_4]^{2-}$, 333 $[Fe_4(N^tBu)_2Se_2Cl_4]^{2-}$.

Physical Measurements. NMR spectra were obtained on Bruker Avance 300 MHz spectrometers at ca. 22 °C, with chemical shifts reference to residual protiosolvent signals. Solution absorption spectra were recorded using a Varian Cary 5000 UV−vis−NIR spectrophotometer; concentrated solutions and short path length (0.1 mm) cells were used to minimize decomposition from trace contaminants. Mössbauer spectra were collected on polycrystalline samples using instrumentation described elsewhere,[39] with data processed and simulated using Igor Pro (WaveMetrics, Inc., Portland, OR, USA). Electrochemical measurements were conducted inside a N_2 atmosphere glovebox according to reported procedures[39] using a Biologic SP-150 potentiostat; redox potentials were referenced using ferrocene/ferrocenium as an internal standard and then converted to the SCE scale for comparison against literature data. EPR spectra were recorded on modified Varian E-4 (X-band, 14 K) and E-109 (Q-band, 35 GHz, 2 K) spectrometers. The Q-band spectrometer employed a liquid He immersion dewar so that spectra were measured under "passage" conditions to yield an absorption line shape; a digital derivative spectrum is shown in Figure 8 to facilitate comparison against conventional EPR spectral presentations. Elemental analyses were performed by Midwest Microlab, LLC (Indianapolis, IN) or by Oneida Research Services, Inc. (Whitesboro, NY). Negative-ion nanoelectrospray ionization mass spectrometry (ESI-MS) was conducted using a Waters/Micromass QTOF Ultima Global mass spectrometer; samples were infused at 1 μL/min in dry MeCN, and the following operation conditions were employed: source temperature = 80 °C, capillary voltage = 3 kV, cone voltage = 65−165 V, collision energy = 3−10 eV, and mass resolution = ~8000.

X-ray Crystallography. Crystals suitable for diffraction analysis were obtained from storage of concentrated *n*-pentane solutions (**6** as green parallelepiped rods; **7** as black blocks), by *n*-pentane/HMDSO vapor diffusion (**7-Se** as black blocks), or by $MeCN/Et_2O$ vapor diffusion (**2**, **8**, **10**, and **10-Se** as black blocks; **9** as black plates), all at low temperatures (−20 to −30 °C).

Data were collected using Mo Kα radiation on a either a Nonius KappaCCD diffractometer equipped with an MSC X-stream cryosystem or a Bruker SMART APEX diffractometer with an Oxford 700 Series Cryostream Cooler. Data sets were collected, indexed, and processed using Nonius DENZO-SMN/SCALEPACK or Bruker APEX2 software suites, and structures were solved and refined using Bruker SHELXTL (v5.04 or 6.14). Essential crystallographic data are summarized in Table 6, with specific details for individual structure determinations available separately in CIF format as Supporting Information.

■ ASSOCIATED CONTENT

Ⓢ Supporting Information

Crystallographic data in CIF format and structural figures for selenium-substituted clusters **7-Se** and **10-Se**. This material is available free of charge via the Internet at http://pubs.acs.org.

■ AUTHOR INFORMATION

Corresponding Author

*E-mail: sclee@uwaterloo.ca.

Present Addresses

[†]Department of Chemistry and Chemical Biology, Harvard University, Cambridge, MA 02318, United States.

[‡]Department of Atmospheric Science and Chemistry, Plymouth State University, Plymouth, NH 03264, United States.

Notes

The authors declare no competing financial interest.

■ ACKNOWLEDGMENTS

This research was supported by NSERC, CFI, ORF, and, for initial studies, the U.S. National Science Foundation (CAREER CHE-9984645). We thank L. L. Tan, Dr. J. Assoud, and Dr. R. W. Smith (Waterloo) for experimental, crystallographic, and mass spectrometric assistance, respectively, Prof. J. Telser (Roosevelt) for EPR measurements and helpful discussions, and Profs. B. M. Hoffman (Northwestern) and R. H. Holm (Harvard) for access to EPR and Mössbauer spectrometers, respectively.

■ REFERENCES

(1) Burgess, B. K.; Lowe, D. J. *Chem. Rev.* **1996**, *96*, 2983−3012.

(2) Eady, R. R. *Chem. Rev.* **1996**, *96*, 3013−3030.

(3) Seefeldt, L. C.; Hoffman, B. M.; Dean, D. R. *Annu. Rev. Biochem.* **2009**, *78*, 701−722.

(4) Einsle, O.; Tezcan, F. A.; Andrade, S.; Schmid, B.; Yoshida, M.; Howard, J. B.; Rees, D. C. *Science* **2002**, *297*, 1696.

(5) Howard, J. B.; Rees, D. C. *Proc. Natl. Acad. Sci. U.S.A.* **2006**, *103*, 17088−17093.

(6) Seefeldt, L. C.; Dance, I. G.; Dean, D. R. *Biochemistry.* **2004**, *43*, 1401−1409.

(7) Igarashi, R. Y.; Seefeldt, L. C. *Crit. Rev. Biochem. Mol. Biol.* **2003**, *38*, 351−384.

(8) Christiansen, J.; Dean, D. R.; Seefeldt, L. C. *Ann. Rev. Plant Physiol. Plant Mol. Biol.* **2001**, *52*, 269−295.

(9) Harris, T. V.; Szilagyi, R. K. *Inorg. Chem.* **2011**, *50*, 4811−4824.

(10) Vrajmasu, V.; Munck, E.; Bominaar, E. L. *Inorg. Chem.* **2003**, *42*, 5974−5988.

(11) Hinnemann, B.; Nørskov, J. K. *J. Am. Chem. Soc.* **2003**, *125*, 1466−1467.

(12) Lovell, T.; Liu, T. Q.; Case, D. A.; Noodleman, L. *J. Am. Chem. Soc.* **2003**, *125*, 8377−8383.

(13) Schimpl, J.; Petrilli, H. M.; Blöchl, P. E. *J. Am. Chem. Soc.* **2003**, *125*, 15772−15778.

(14) (a) Dance, I. *Chem. Commun.* **2003**, 324−325. (b) Dance, I. *Inorg. Chem.* **2006**, *45*, 5084−5091.

(15) (a) Lee, H.-I.; Benton, P. M. C.; Laryukhin, M.; Igarashi, R. Y.; Dean, D. R.; Seefeldt, L. C.; Hoffman, B. M. *J. Am. Chem. Soc.* **2003**, *125*, 5604−5605. (b) Yang, T.-C.; Maeser, N. K.; Laryukhin, M.; Lee, H.-I.; Dean, D. R.; Seefeldt, L. C.; Hoffman, B. M. *J. Am. Chem. Soc.* **2005**, *127*, 12804−12805. (c) Lukoyanov, D.; Pelmenschikov, V.; Maeser, N.; Laryukhin, M.; Yang, T. C.; Noodleman, L.; Dean, D. R.; Case, D. A.; Seefeldt, L. C.; Hoffman, B. M. *Inorg. Chem.* **2007**, *46*,

11437−11449. (d) Pelmenschikov, V.; Case, D. A.; Noodleman, L. *Inorg. Chem.* **2008**, *47*, 6162−6172.
(16) Lancaster, K. M.; Roemelt, M.; Ettenhuber, P.; Hu, Y.; Ribbe, M. W.; Neese, F.; Bergmann, U.; DeBeer, S. *Science* **2011**, *334*, 974−977.
(17) Spatzal, T.; Aksoyoglu, M.; Zhang, L.; Andrade, S. L. A.; Schleicher, E.; Weber, S.; Rees, D. C.; Einsle, O. *Science* **2011**, *334*, 940.
(18) Kastner, J.; Hemmen, S.; Blöchl, P. E. *J. Chem. Phys.* **2005**, *123*, 074306.
(19) Huniar, U.; Ahlrichs, R.; Coucouvanis, D. *J. Am. Chem. Soc.* **2004**, *126*, 2588−2601.
(20) Cao, Z.; Zhou, Z.; Wan, H.; Zhang, Q.; Thiel, W. *Inorg. Chem.* **2003**, *42*, 6986−6988.
(21) (a) Dance, I. *Dalton Trans.* **2008**, 5977−5991. (b) Dance, I. *Dalton Trans.* **2008**, 5992−5998. (c) Dance, I. *Dalton Trans.* **2012**, *41*, 4859−4865.
(22) Peters, J. W.; Szilagyi, R. K. *Curr. Opin. Chem. Biol.* **2006**, *10*, 101−108.
(23) (a) Hoffman, B. M.; Dean, D. R.; Seefeldt, L. C. *Acc. Chem. Res.* **2009**, *42*, 609−619. (b) Dos Santos, P. C.; Igarashi, R. Y.; Lee, H.-I.; Hoffman, B. M.; Seefeldt, L. C.; Dean, D. R. *Acc. Chem. Res.* **2005**, *38*, 208−214.
(24) (a) Lee, S. C.; Holm, R. H. *Chem. Rev.* **2004**, *104*, 1135−1157. (b) Malinak, S. M.; Coucouvanis, D. *Prog. Inorg. Chem.* **2001**, *49*, 599−662.
(25) Lee, S. C.; Holm, R. H. *Proc. Natl. Acad. Sci. U.S.A.* **2003**, *100*, 3595−3600.
(26) (a) Wolff, T. E.; Berg, J. M.; Warrick, C.; Hodgson, K. O.; Holm, R. H.; Frankel, R. B. *J. Am. Chem. Soc.* **1978**, *100*, 4630−4632. (b) Wolff, T. E.; Berg, J. M.; Hodgson, K. O.; Frankel, R. B.; Holm, R. H. *J. Am. Chem. Soc.* **1979**, *101*, 4140−4150.
(27) Kim, J. S.; Rees, D. C. *Science* **1992**, *257*, 1677−1682.
(28) (a) Ohki, Y.; Ikagawa, Y.; Tatsumi, K. *J. Am. Chem. Soc.* **2007**, *129*, 10457−10465. (b) Hashimoto, T.; Ohki, Y.; Tatsumi, K. *Inorg. Chem.* **2010**, *49*, 6102−6109.
(29) (a) Hlavinka, M. L.; Miyaji, T.; Staples, R. J.; Holm, R. H. *Inorg. Chem.* **2007**, *46*, 9192−9200 and references therein. (b) Zhang, Y.; Zuo, J. -L.; Zhou, H.-C.; Holm, R. H. *J. Am. Chem. Soc.* **2002**, *124*, 14292−14293.
(30) (a) Pryadun, R.; Holm, R. H. *Inorg. Chem.* **2008**, *47*, 3366−3370. (b) Rao, P. V.; Bhaduri, S.; Jiang, J.; Hong, D.; Holm, R. H. *J. Am. Chem. Soc.* **2005**, *127*, 1933−1945. (c) Koutmos, M.; Coucouvanis, D. *Angew. Chem., Int. Ed.* **2004**, *43*, 5023−5025. (d) Zhang, Y.; Holm, R. H. *Inorg. Chem.* **2004**, *43*, 674−682. (e) Chen, C.; Cai, J.; Liu, Q.; Wu, D.; Lei, X.; Zhao, K.; Kang, B.; Lu, J. *Inorg. Chem.* **1990**, *29*, 4878−4881. (f) Cai, J.-H.; Chen, C.-N.; Liu, Q.-T.; Zhuang, B.-T.; Kang, B.-S.; Lu, J.-X. *Chin. J. Struct. Chem.* **1989**, *8*, 220. (g) Osterloh, F.; Saak, W.; Pohl, S.; Meier, C.; Trautwein, A. X. *Inorg. Chem.* **1998**, *37*, 3581−3587. (h) Hagen, K. S.; Christou, G.; Holm, R. H. *Inorg. Chem.* **1983**, *22*, 309−314. (i) Henkel, G.; Tremel, W.; Krebs, B. *Angew. Chem., Int. Ed.* **1981**, *20*, 1033−1034.
(31) (a) Ohki, Y.; Imada, M.; Murata, A.; Sunada, Y.; Ohta, S.; Honda, M.; Sasamori, T.; Tokitoh, N.; Katada, M.; Tatsumi, K. *J. Am. Chem. Soc.* **2009**, *131*, 13168−13178. (b) Ohki, Y.; Sunada, Y.; Honda, M.; Katada, M.; Tatsumi, K. *J. Am. Chem. Soc.* **2003**, *125*, 4052−4053.
(32) Zhang, Y.; Holm, R. H. *Inorg. Chem.* **2004**, *43*, 674−682.
(33) (a) Berlinguette, C. P.; Holm, R. H. *J. Am. Chem. Soc.* **2006**, *128*, 11993−12000. (b) Zhang, Y.; Holm, R. H. *J. Am. Chem. Soc.* **2003**, *125*, 3910−3920. (c) Zheng, B.; Chen, X.-D.; Zheng, S.-L.; Holm, R. H. *J. Am. Chem. Soc.* 2012, *134*
(34) Han, J.; Koutmos, M.; Ahmad, S. A.; Coucouvanis, D. *Inorg. Chem.* **2001**, *40*, 5985−5999.
(35) Deng, L.; Majumdar, A.; Lo, W.; Holm, R. H. *Inorg. Chem.* **2010**, *49*, 11118−11126.
(36) Chen, X.-D.; Duncan, J. S.; Verma, A. K.; Lee, S. C. *J. Am. Chem. Soc.* **2010**, *132*, 15884−15886.
(37) Kovacs, J. A.; Holm, R. H. *J. Am. Chem. Soc.* **1986**, *108*, 340−341.
(38) (a) Cui, Z.; Henderson, R. A. *Transition Met. Chem.* **2006**, *31*, 530−540. (b) Cui, Z.; Henderson, R. A. *Inorg Chem.* **2002**, *41*, 4158−4166.
(39) Duncan, J. S.; Nazif, T. M.; Verma, A. K.; Lee, S. C. *Inorg. Chem.* **2003**, *42*, 1211−1224.
(40) Duncan, J. S.; Zdilla, M. J.; Lee, S. C. *Inorg. Chem.* **2007**, *46*, 1071−1080.
(41) Comparative pK_a values for relevant protonated N-anion donors in organic solvents. (a) NH_3, ∼41; pyrrolidine, ∼44 (DMSO): Bordwell, F. G.; Drucker, G. E.; Fried, H. E. *J. Org. Chem.* **1981**, *46*, 632−635. (b) $^{i}Pr_2NH$, 35.7 (THF): Fraser, R. R.; Mansour, T. S. *J. Org. Chem.* **1984**, *49*, 3443; Also, see correction: *J. Org. Chem.* **1984**, *49*, 5284. (c) $(Me_3Si)_2NH$, 26 (THF): Fraser, R. R.; Mansour, T. S.; Savard, S. *J. Org. Chem.* **1985**, *50*, 3232−3234.
(42) (a) Wong, G. B.; Bobrik, M. A.; Holm, R. H. *Inorg. Chem.* **1978**, *17*, 578−584. (b) Bobrik, M. A.; Hodgson, K. O.; Holm, R. H. *Inorg. Chem.* **1977**, *16*, 1851−1858. (c) Do, Y.; Simhon, E. D.; Holm, R. H. *Inorg. Chem.* **1983**, *22*, 3809−3812.
(43) Courtois, G.; Miginiac, L. *Tetrahedron Lett.* **1987**, *28*, 1659−1660.
(44) (a) Andersen, R. A.; Faegri, K.; Green, J. C.; Haaland, A.; Lappert, M. F.; Leung, W. P.; Rypdal, K. *Inorg. Chem.* **1988**, *27*, 1782−1786. (b) Olmstead, M. M.; Power, P. P.; Shoner, S. C. *Inorg. Chem.* **1991**, *30*, 2547−2551.
(45) Ebels, J.; Spirk, S.; Pietschnig, R. A Facile Lab Scale Synthesis of Red Selenium. *10th International Electronic Conference on Synthetic Organic Chemistry (ECSOC-10)*; MDPI: Basel, 2006, http://www.usc.es/congresos/ecsoc/10/SST/d002/d002.pdf (accessed Oct 14, 2011).
(46) Ohki, Y.; Sunada, Y.; Tatsumi, K. *Chem. Lett.* **2005**, *34*, 172−173.
(47) Rao, P. V.; Holm, R. H. *Chem. Rev.* **2004**, *104*, 527−559.
(48) Zdilla, M. J.; Verma, A. K.; Lee, S. C. *Inorg. Chem.* **2011**, *50*, 1551−1562.
(49) (a) Verma, A. K.; Nazif, T. N.; Achim, C.; Lee, S. C. *J. Am. Chem. Soc.* **2000**, *122*, 11013−11014. (b) Link, H.; Decker, A.; Fenske, D. Z. *Anorg. Allg. Chem* **2000**, *626*, 1567−1574.
(50) Schaumann, E.; Wriede, U.; Ehlers, J. *Synthesis* **1980**, 907−908.
(51) In the preparation of **11**, chloride/thiolate metathesis was achieved using 5% excess pivaloyl chloride in place of the 100% excess benzoyl chloride specified in ref 42a.
(52) Prepared analogously to $[Fe_4S_4Cl_4]^{2-}$ (refs 42a and 51) using $(Et_4N)_2[Fe_4Se_4(SEt)_4]$: Yu, S. B.; Papaefthymiou, G. C.; Holm, R. H. *Inorg. Chem.* **1991**, *30*, 3476−3485.
(53) Rh(I): (a) Pechmann, T.; Brandt, C. D.; Werner, H. *Chem. Commun.* **2003**, 1136−1137. (b) Schwab, P.; Wolf, J.; Mahr, N.; Steinert, P.; Herber, U. *Chem.—Eur. J.* **2000**, *6*, 4471−4478. (c) Schwab, P.; Mahr, N.; Wolf, J.; Werner, H. *Angew. Chem., Int. Ed.* **1994**, *33*, 97−99.
(54) Cu(I,II): (a) Lobana, T. S.; Khanna, S.; Butcher, R. J.; Hunter, A. D.; Zeller, M. *Inorg. Chem.* **2007**, *46*, 5826−5828. (b) Horn, C.; Dance, I.; Craig, D.; Scudder, M.; Bowmaker, G. *J. Am. Chem. Soc.* **1998**, *120*, 10549−10550.
(55) Ag(I): Noguchi, R.; Sugie, A.; Okamoto, Y.; Hara, A.; Nomiya, K. *Bull. Chem. Soc. Jpn.* **2005**, *78*, 1953−1962.
(56) Cd(II): (a) Mallela, S. P.; Schwan, F.; Geanangel, R. A. *Inorg. Chem.* **1996**, *35*, 745−748. (b) Daoud, A. *Bull. Soc. Chim. Fr.* **1976**, 1418.
(57) A symmetric amide bridge (mean Fe−N bond length = 2.00(1) Å) is known in one mixed-valent Fe(II)/Fe(III) complex: Takemoto, S.; Ogura, S.-I.; Yo, H.; Hosokoshi, Y.; Kamikawa, K.; Matsuzaka, H. *Inorg. Chem.* **2006**, *45*, 4871−4873.
(58) Hexacoordinate effective ionic radii, Se^{2-} = 1.98 Å, S^{2-} = 1.84 Å: Shannon, R. D. *Acta Crystallogr. Sect. A: Found. Crystallogr* **1976**, *32*, 751−767.
(59) (a) Chu, C. T.-W.; Gall, R. S.; Dahl, L. F. *J. Am. Chem. Soc.* **1982**, *104*, 737−746. (b) Gall, R. S.; Chu, C. T.-W.; Dahl, L. F. *J. Am. Chem. Soc.* **1974**, *96*, 4019−4023.
(60) Vela, J.; Cirera, J.; Smith, J. M.; Lachicotte, R. J.; Flaschenriem, C. J.; Alvarez, S.; Holland, P. L. *Inorg. Chem.* **2007**, *46*, 60−71.

(61) Initial results: Lancaster, K. M.; Tan, L. L.; Zhang, W.; Pollock, C. J.; Lee, S. C.; DeBeer, S. Manuscript in preparation.
(62) Sharp, C. R.; Duncan, J. S.; Lee, S. C. *Inorg. Chem.* **2010**, *49*, 6697−6705.
(63) Christou, G.; Ridge, B.; Rydon, H. N. *J. Chem. Soc., Dalton Trans.* **1978**, 1423−1425.
(64) Scott, T. A.; Berlinguette, C. P.; Holm, R. H.; Zhou, H. C. *Proc. Natl. Acad. Sci. U.S.A.* **2005**, *102*, 9741−9744.
(65) Papaefthymiou, V.; Millar, M. M.; Münck, E. *Inorg. Chem.* **1986**, *25*, 3010−3014.